China University of Geosciences
College of Marine Science and Technology
School of Earth Sciences
Email: jerryqdc@gmail.com, js-wang@cug.edu.cn

Biogeosciences

Date: October 8, 2018

Subject: Post-Review Revision of Manuscript bg-2018-340

Dear Professor Treude,

Thank you for handing our manuscript—Vivianite formation in methane-rich deep-sea sediments from the South China Sea—for consideration for publication in *Biogeosciences*. We received two generally positive reviews from the solicited reviewers whose efforts, we believe, have helped to clarify and improve the quality of the revised manuscript. Accordingly, where possible we have followed the reviewers' recommendations and amended the manuscript.

Since the initial submission, by mutual consent, we have opted to exchange the order of the second and third authors. Hereby we submit the revised manuscript bg-2018-340 with the full consent of the named authors (Jiarui Liu, Gareth Izon, Jiasheng Wang, Gilad Antler, Zhou Wang, Jie Zhao and Matthias Egger). All the authors declare that the work is their own, it is not under consideration elsewhere, and it is not compromised via any confliction.

With this letter, we append the initial comments from each reviewer (orange), followed by our response (black). We include an explanation of how and where each point raised by the reviewers was incorporated into the manuscript alongside a highlighted manuscript to explicitly locate our changes.

Yours sincerely,

Jiarui Liu and Jiasheng Wang

on behalf of all named co-authors

Response to the Reviewers: Manuscript bg-2018-340

Reviewer 1: We thank Dr. März for his comments and insight. His requests have helped to clarify the text and highlight omissions from our initial submission. We reply to each of his comments in turn and revise the manuscript accordingly.

R1.1). Comment (sampling of sediments): It is unclear from the text (Methods) how the core sections were processed after sectioning. They were transferred into cool storage. What happened next? Were the sections split on board and samples taken immediately? Were samples stored frozen and/or anoxic to avoid pyrite oxidation prior to freeze-drying? This is crucial for the determination of reactive Fe fractions. Sampling of pore waters: Were pore waters extracted using rhizons? Were they extracted from the closed core by drilling holes into the liner, or were they extracted from the split core surfaces? How long before pore water sampling were the sections split? This is crucial not only for methane and sulphate concentrations, but for any volatile and/or redox sensitive species, i.e., Fe^{2+}, HS^-, HPO_4^{2-}. For example, pore water Fe^{2+} could precipitate as Fe (oxyhydr)oxides and adsorb pore water HPO_4^{2-}.

Reply: We acknowledge this initial oversight and agree that more detail should be included to clarify how the sediments/pore waters were handled and collected.

With respect to core handling, after sectioning on board, the cores were stored below 4 °C. The sections were then split and subsampled immediately after the cruise. Sub-samples were stored frozen (−20 °C) prior to freeze-drying to minimize pyrite oxidation. The obvious peak of Fe-oxides at ~900 cm depth (Fig. 8a) may include part of acid volatile sulfur (AVS) pool since AVS oxidizes to dithionite- and oxalate-extractable Fe phases during freeze-drying or exposure to air. It is difficult to quantify the influence of pyrite oxidation on the reactive Fe distributions at Site 973-4 but we anticipate this to be minimized via our sample handling. The clarifying text can be found in the amended manuscript on lines 16–19 on page 4. Acknowledgement of potential post-recovery oxidation can now be found on lines 7–9 on page 8. This was included in the initial submission.

Unfortunately, the pore waters from Site 973-4 were not immediately extracted; instead, they were extracted several months later via centrifugation of previously frozen sub-samples. Consequently, the pore water chemistry of Site 973-4 (Fig. 2b) is more likely to reflect post-recovery oxidation or contamination rather than sediment-housed processes. For example, volatile sulfide loss and/or sulfide oxidation could have modified the distribution of sulfur species. Alternatively, as R1 suggests, precipitation of dissolved Fe could influence the distributions of Fe-sensitive species. It is for this reason that we opted to deemphasize the importance of the published pore water chemistry in favor of data

derived from proximal sites (Fig. 2b; see R1.2). A clarifying paragraph beginning on line 23 (page 5) has been added detailing how the pore water data from the surrounding sites was generated.

R1.2). Comment (pore water data and SMTZ definition): In general, I am not sure if I trust the practice of inferring pore water geochemistry from neighboring sites, especially since no further information is provided about these. How far away are these nearby sites, and were they affected by the same paleo-depositional processes as the study site? Are there distinct similarities in lithology, sedimentation rates etc. that would warrant the "import" of pore water data from these sites? Some of this information can be extracted/inferred from Figure 2 but should be explained in the text as well. From each of the nearby sites, there are only 1–2 methane data points available just below the SMTZ. It should be highlighted in the text that (whether?) this is sufficient to define the SMTZ position. I would also shift the upper boundary of the SMTZ upwards, to the depth where the first methane-free sample was encountered. Also, the methods of pore water sampling and data generation at these nearby sites should be explained.

Reply: We agree with R1's concerns but, given the complications concerning the quality of the pore water data at Site 973-4 (See R1.1), we believe that synthesizing pore water data from the surrounding sites is likely to be more representative. We stress that we do not advocate this approach to replace pore water analysis but, in its absence, we argue that pore water data from nearby sites when combined with solid-phase distributions from Site 973-4 allow us to estimate an approximate position of the SMTZ with sufficient accuracy for the purposes of our manuscript.

Sites from which we obtained pore water data are separated from Site 973-4 by a few kilometers. These sites are lithologically similar and dominated by silty clay. Unfortunately, age constraints and sedimentation rates are lacking at the other sites. The pore water chemistry from the combined sites, however, is analogous, indicating that each site was likely affected by the same depositional process(es). Solid phase distributions at Site 973-4 support this inference. At the sulfidization front, sulfide is known to diffuse out of the SMTZ promoting reductive dissolution of Fe-oxides and the sequestration of elemental sulfur and Fe monosulfides ($3H_2S + 2FeOOH \rightarrow S^0 + 2FeS + 4H_2O$). At Site 973-4 there are two pronounced peaks of elemental sulfur at 730 and 880 cm depth (Liu et al., In prep), while AVS concentrations reach their maximum at ~900 cm depth (Fig. 9b). Accordingly, we combine these site-specific solid-phase records, with the "imported" pore water data to infer the SMTZ is currently around 700–880 cm depth at Site 973-4. As R1 suggested, however, the first methane-free samples appear at 640 cm depth. Considering the first elemental sulfur peak at 730 cm depth, we stress that it is more appropriate to define the upper boundary of the SMTZ as a rough depth for the purposes of our manuscript, i.e. around 700 cm depth.

Given following discussion, and the need to draw on the data of others, we agree with R1 that the pertinent details of pore water sampling and analysis should also be included in the manuscript. Clarifying text to rectify this oversight begins on line 23, page 5. The new text reads: Pore water extraction from Site DH-CL11 was conducted on shore via

centrifugation, exploiting sample aliquots that had been immediately taken and stored under vacuum at −80 °C (Lin et al., 2017). Pore water samples from Site B and Site HD319 were collected immediately after recovery by vacuum extraction (Lu et al., 2012; Ye et al., 2016). At each site, the pore water sulfate contents were determined by ion chromatography; whereas, pore water methane concentrations were determined via sediment plug sampling and gas chromatographic analysis of the resultant headspace gas (Lin et al., 2017; Lu et al., 2012; Ye et al., 2016).

R1.3). Comment (iron extraction): Please cite a reference that defines Fe phases extracted by an anoxic 0.5M HCl solution. I am not actually sure this extraction method has been well calibrated using different Fe minerals.

Reply: The anoxic 0.5 M HCl extraction was adopted from Holmkvist et al. 2011 and 2014 (GCA). More than 97% of amorphous iron (hydro)oxides and ferrihydrite can be extracted, while other Fe-oxides minerals are apparently recalcitrant to this extractant (Wallmann et al., 1993, Limnology and Oceanography; Haese et al., 1997, GCA). Compared to the more well-known dithionite method (e.g. Poulton and Canfield, 2005), the HCl method has not been well calibrated. We added the omitted references on line 31–32 of page 4. An additional sentence has also been added on line 9–11 page 5.

R1.4). Comment (appropriate description of methods): Lots of data are shown (AVS, pyrite, S isotopes, Fe-bound P, Ca-P etc.) that are not covered in the Methods section at all. Even if they were published before, a brief account of how these data were generated is required in this manuscript. Were the analyses conducted on splits of exactly the same samples, or nearby samples, or were samples taken at different times? I would also defer from making speculations about what certain data would look like if they had been generated (e.g., pore water HPO_4^{2-}).

Reply: Following R1's advice, a brief description of how the various published datasets were generated has been included in the amended manuscript. The new paragraph is found on line 31, page 5, which reads: Previously published data was determined using separate aliquots of the same subsamples exploited herein. This earlier work followed established protocols and full methodological details are provided in the respective papers. Accordingly, only a brief description is provided here. Acid volatile sulfide was liberated via HCl distillation and trapped by zinc acetate, its concentration was then determined spectrophotometrically (Zhang et al., 2014). Pyrite aggregates were handpicked from the coarse-fraction (> 65 μm) with its abundance expressed relative to the coarse grains. The sulfur isotopic composition of handpicked pyrite was determined directly via flash combustion using a Delta V Plus isotope ratio mass spectrometer (IRMS; Lin et al., 2015). The solid-phase distribution of P was revealed through the SEDEX sequential extraction scheme (Ruttenberg, 1992). Fe-bound P and authigenic carbonate fluorapatite were extracted by citrate-bicarbonate-dithionite and Na-acetate buffer, respectively (Zhang et al., 2018b). The carbon isotopic composition of total inorganic carbon was determined after treatment with phosphoric acid using a Finnigan MAT-252 IRMS (Ou, 2013; Zhang et al., 2018c). Finally, magnetic susceptibility data was generated using a MFK1-FA kappameter (Lin et al., 2017a).

All analyses were conducted on aliquots of the same sample powder, ensuring the data are comparable. As detailed on line 17–19, page 4, subsamples of the core were split into two and the second aliquot was homogenized for chemical analysis. Although the analyses were made at different times, the powdered samples were kept frozen to minimize oxidation.

Following R1's advice, speculative aspects have been removed from the amended manuscript.

R1.5). Comment (the Ca-P fraction): A lot of Ca-P is found below the SMTZ, more than Fe-bound P. This is not discussed sufficiently. Is part of the HPO_4^{2-} that is (tentatively) liberated in the SMTZ precipitated as authigenic apatite? Is this supported by pore water Ca and F profiles (if not at this site, maybe at the nearby sites)? And could the formation of Ca-P be related to the sulphidisation front that consumed part of the Fe-AOM-derived Fe^{2+} and precipitated it as AVS? In other words, does the activity of a sulphidisation front put a constraint on how much Fe(II) phosphate can precipitate below the SMTZ? Are there any estimates of the kinetics of these potentially competing authigenic processes of Fe^{2+} removal from the sub-SMTZ pore waters? This would be very interesting, as it would allow to better link the rate of HS^- production in the SMTZ (which is largely controlled by sulphate diffusion from above and methane delivery from below), the amount of reactive Fe oxides beneath the SMTZ, and the potential to form different authigenic P phases beneath the SMTZ.

Reply: This is an interesting point, and one that warrants inclusion in the discussion of the amended manuscript, albeit still speculative due to the lack of appropriate data. We have added an extra section to the manuscript (*Long-term vivianite preservation—An outstanding question*) on page 14 which includes the following points:

As pointed out by R1, authigenic Ca-P is the major P sink at Site 973-4 (~55%), in agreement with its globally estimated importance. Indeed, Ca-P concentrations are much higher than Fe-bound P throughout the studied core. It is well known that a steady supply of phosphate, fueled by the reductive dissolution of Fe-oxides, fosters thermodynamically favorable conditions capable of promoting apatite authigenesis in proximity to the SMTZ (Egger et al., 2015a, Fig. S8; März et al., 2018). Thus, as suggested by R1, it is possible that some of the SMTZ-sourced phosphate is consumed and precipitated as authigenic apatite, providing the other necessary chemical constituents are available. While there are no reliable pore water data from Site 973-4 (R1.1), dissolved Ca^{2+} concentrations from Site B are consistent with ongoing apatite authigenesis, with a linear down-core decrease from the sediment-water interface to the upper part of the SMTZ (12.5–2.5 mM) where most of the Ca^{2+} has been consumed (Ye et al., 2016). To our knowledge, however, there are no available dissolved F^- and PO_4 data to unequivocally confirm apatite precipitation rather than other calcium-harboring phases.

Vivianite formation below the SMTZ depends on PO_4 and Fe^{2+} availability, which we suggest are mainly supplied from PO_4 liberation in the SMTZ and the upward flux of Fe^{2+} from iron reduction at depth. Kinetics notwithstanding, providing

there is sufficient Ca^{2+} and F^{-}, apatite will remove PO_4 competing and effectively limiting vivianite precipitation. At Site 973-4 vivianite occurs below ~920 cm depth suggesting that even if apatite authigenesis is a competing process, Ca^{2+} and F^{-} have likely been consumed at this depth. Importantly, vivianite authigenesis occurs below the sulfidization front (~900 cm) implying that FeS precipitation is kinetically favored relative to vivianite precipitation immediately below the SMTZ. We speculate, therefore, that the pore water chemistry and the activity of sulfidization front will influence the depth of vivianite formation. Intensified activity at the sulfidization front would liberate more phosphate, however, the extra sulfide flux may serve to nullify the ascent of Fe^{2+} from depth, especially as highly reactive iron is consumed, preventing vivianite formation, or forcing it deeper into the sediment-pile.

Unfortunately, we do not have the data to definitively test the hypothesized competing role of apatite and FeS authigenesis in vivianite precipitation. However, any process that serves to deplete pore water PO_4 and Fe^{2+} will hypothetically compete with vivianite formation. Future work in/around the study area should focus on generating comprehensive pore water and solid phase data sets, which when coupled with reactive transport models, will better link the rate of HS^{-} production in the SMTZ, the amount of reactive Fe-oxides beneath the SMTZ, and the potential to form different authigenic P phases.

R1.6). Comment ("deepening" of the SMTZ): The suggestion of a previously shallower SMTZ in section 5.1 comes out of the blue, without any specific reasoning for why the authors think this was the case. I do not necessarily disagree with this hypothesis, but the authors need to give some supporting arguments, e.g., maybe the fact that pyrite exists above the SMTZ (although this could also be formed by organoclastic sulphate reduction). They then need to better develop how such a deepening of the SMTZ would have affected all the described geochemical parameters, and if observations agree with expectations. Finally, they need to relate the migration to the SMTZ to depositional/environmental processes – if it was not caused by changes in sedimentation rate, was it changes in methane flux from below?

Reply: If we accept that the current SMTZ is around 700–880 cm depth based on the arguments presented in R1.2, we can speculate on the evolution of the SMTZ at Site 973-4. The preservation of Fe-oxides and absence of pyrite below the SMTZ were most likely caused by the rapid upward migration of the SMTZ from below 14m (i.e. deeper than the core) to middle of our record. The resultant short exposure of Fe-oxide minerals to sulfidic conditions led to incomplete reduction and sulfidization of the reactive iron pool (März et al., 2018). After its ascent, the SMTZ apparently stabilized around 560–880 cm, leaving pronounced imprints in the pyrite, Fe-oxide, Fe-silicate, total inorganic carbon and magnetic susceptibility profiles (Figs. 7–9). It should be noted that pyrite formed by organoclastic sulfate reduction usually features more negative $\delta^{34}S$ values (−50‰) such as those seen at ~300–560 cm depth. Whereas, the $\delta^{34}S$ excursion seen at ~560–880 cm depth is best explained by sulfate driven AOM at and above the current SMTZ. Assimilating these observations,

we suggest that the SMTZ might have slowly migrated downward from ~560–700 cm to its current position at ~700–880 cm depth.

This migration pattern may explain why we observed vivianite at 747 cm depth (Fig. 6). The paleo-SMTZ may have been shallower (e.g. ~560–700 cm depth) allowing vivianite to precipitate at shallower depths (e.g. 747 cm depth). We speculate that most of the vivianite formed at/around the current SMTZ was readily converted to Fe-sulfide phases via reaction with H_2S during the subsequent downward migration of the SMTZ, concentrating vivianite below the current SMTZ. Consequently, if the SMTZ continued to descend within the sediment pile, we would expect that the pronounced solid-phase imprints observed at ~560–880 cm would also descend to sediments below the current SMTZ.

Given the largely invariant sedimentation rate at Site 973-4 over the duration of the core (Fig. 2a), we hypothesize that the migration history of the SMTZ was driven by changes in the methane flux. During the sea-level low stand during the Last Glacial Maximum, the resulting low hydrostatic pressure would have destabilized any underlying methane clathrates, enhancing methane fluxes while promoting a rapid upward migration of the SMTZ (Borowski et al., 1996). The subsequent Holocene sea-level rise, however, would have had the opposite effect, diminishing methane fluxes and instigating the slow downward migration of the SMTZ to its current position. Our observations are consistent with those of others who suggest that the SMTZ needs to be static (i.e. ~560–880 cm depth) for thousands of years to allow the development of significant authigenic Fe(II) phosphate mineral enrichments below the SMTZ (März et al., 2018).

The manuscript has been substantially modified to discuss the evolution of the SMTZ at Site 973-4. These amendments are mainly in Section 5.1 (page 8). Specifically, among the addition of a few additional sentences, we have added an extra paragraph beginning on line 21 page 9 to expand on the evidence for SMTZ migration and our favored driving mechanism. Toward the end of the following paragraph we have introduced the consequences of SMTZ migration on the solid-phase geochemical records.

R1.7). Comment (missing reference): Please cite März et al. (2008, 2018; Marine Geology) when stating that a lot of the vivianite is likely finely disseminated. In general, wherever the authors speculate about the wide-spread occurrence of vivianite in methane-rich continental margin sediments, they need to cite the new study by März et al. (2018) (Marine Geology) that comes to exactly the same conclusion.

Reply: We apologize for the omission of the reviewer's most recent work. We had submitted our paper before the 2018 study had been formally published. As suggested, in our amended manuscript, we have cited März et al. (2008 and 2018) to fully credit the importance of finely disseminated vivianite in methane-rich continental margin settings.

R1.8). Comment (vivianite to Ca-P sink switching): When looking at the Ca-P profile, one cannot help but notice that there is an increase to higher values from the SMTZ to the bottom of the core, while Fe-P and vivianite seem to decrease

in parallel. This raises the question of the long-term stability of vivianite in the sedimentary record, and its use as paleo SMTZ marker. In fact, vivianite is hardly ever found in older sediments/sedimentary rocks where carbonate fluorapatite is by far the dominant mineral, so there is a strong argument that vivianite is (at least partly) transformed into something else, maybe authigenic apatite?

Reply: The question concerning vivianite's longevity in the sedimentary record is a good one and, indeed, it is an outstanding question that needs to be addressed more generally. Unfortunately, in the context of the available data, we cannot unequivocally answer the posed questions and thus we opted to expand the discussion to encompass the available observations and interpretations. However, given the ambiguity, we also elected to "tone-down" our language to convey uncertainty in the amended manuscript. Again, additional text can be found in the new section included on page 14.

The increase in Ca-P concentrations noted by R1 may reflect the conversion of labile P-species into authigenic apatite—so-called sink switching. Sink switching is considered to be the dominant global process of apatite authigenesis in marine sediments (e.g. Ruttenberg and Berner, 1993; Slomp et al., 1996). Whether vivianite is converted to authigenic apatite at depth, while possible, remains an open question. Moreover, if it were a simple conversion then one would predict a linear increase in apatite with a concomitant decrease in vivianite. Closer inspection of the relevant solid phase records reveals that this is not the case and, in fact, the relationship between apatite and vivianite concentrations is ambiguous, and largely decoupled, at Site 973-4.

Alternatively, the "increase" in authigenic Ca-P from the SMTZ to the bottom of the core may reflect non-vivianite-related apatite authigenesis at depth. Upward fluxes of Ca^{2+} and F^- to the SMTZ have been observed in continental margin settings (e.g. Clemens et al., 2016; März et al., 2018), which would provide the necessary chemical constituents to promote sub-SMTZ apatite authigenesis. As discussed in R1.5, if apatite is a more favorable phosphate sink, then precipitation of this mineral phase could hypothetically curtail vivianite authigenesis. In this scenario, although the two phosphate phases are linked, they are linked through Ca^{2+} (and F^-) availability rather than stability and conversion of one phase to another.

The apparent decrease in vivianite with depth could also be completely decoupled from apatite authigenesis. For example, vivianite is sensitive to oxic conditions, thus it is possible that vivianite in deep-time records has been oxidized to Fe-oxides (e.g., hematite; Berner, 1981), Fe(III) phosphate (e.g., koninckite; März et al., 2008a) or some other unknown phase(s). Pseudomorphs of vivianite are apparently common in the deep-time record, providing at least some evidence for the eventual transformation and stabilization of vivianite (e.g. metavivianite; Rodgers, 1986). Equally, the perceived absence of vivianite in aged sedimentary archives could be an artifact of insufficient surveys. Our work, as well as that of R1 (März et al., 2018), has shown that vivianite is likely a finely disseminated phase and thus may have escaped

detection in many studies. Moreover, typically employed extraction schemes co-extract vivianite, meaning that Fe-P in deep time records could have been wrongly ascribed, and could be vivianite (c.f., März et al., 2008b).

Future work, targeting long cores coupling aqueous- and solid-phase analysis, is required to definitively test our hypotheses linking vivianite authigenesis and Fe-AOM activity, as well as to examine the long-term stability of vivianite in the sedimentary record. More routine application of XRD and modification of solid-phase extraction protocols is also necessary to answer questions relating to the geological significance of vivianite.

R1.9). Comment (importance of findings to the geological past): The link between vivianite formation below the SMTZ in Fe-AOM affected sediments and the potential importance of these processes in the pre-GOE oceans is not well-developed. The actual effects of Fe(II) phosphate formation in an Fe-rich ocean are not discussed at all, only the potential importance of Fe-AOM is mentioned (which is not wrong, but also does not reflect the main story of the research presented here). It would be much more interesting to develop what impact Fe(II) phosphate formation under ferruginous conditions might have had on the marine P cycle. These considerations do not only apply to the pre GOE ocean; as first proposed by März et al. (2008) (GCA) and further developed by Poulton and Canfield (2011) (Elements), ferruginous conditions existed periodically in the Mesozoic (and probably throughout the Phanerozoic) as well. And as März et al. (2008) (GCA) pointed out, the precipitation of Fe(II) phosphates occurred under ferruginous conditions during the deposition of Cretaceous black shales on Demerara Rise, sequestering P from the water column and putting a constraint on the anoxia productivity feedback loop. While we still do not understand enough about the details, and potential effects, of Fe(II) phosphate formation under ferruginous conditions, these earlier studies should be referenced appropriately.

Reply: These are interesting and valid points. We have added clarifying text from line 8 (page 15) to line 2 on the following page. As detailed by R1, the seawater chemistry was vastly different between ancient oceans and their modern counterparts. In our original manuscript, we specifically referred to the predominantly ferruginous state of pre-GOE oceans, yet we concede that ferruginous conditions were also a periodic feature post-GOE oceans as well (März et al., 2008b; Poulton and Canfield, 2011). The latter scenario is subtly different from the former, however, due to ingrowth of the seawater sulfate reservoir (Canfield et al., 2000). Accordingly, we have extended the discussion, fortifying the stance of others while more completely developing our hypotheses concerning the importance of vivianite, and its wider role in P-cycling in ancient oceans.

Where basal waters are oxygenated, we expect a similar pore water pattern to that observed at Site 973-4 or other modern open marine settings (Fig. 10), where vivianite is dominantly formed below the SMTZ. If oxygen concentrations drop, however, vivianite authigenesis is expected to be different with implications for P-cycling and productivity. These intricacies, however, remain to be fully explored.

Under ferruginous (anoxic and Fe^{2+}-rich) conditions dissolved phosphate would be adsorbed to and/or co-precipitated with Fe-oxides (März et al., 2008b), or even precipitated as vivianite directly if Fe^{2+} and PO_4 concentrations were sufficiently high (Dijkstra et al., 2018b). This P shuttle is (at least) partially eradicated if euxinic conditions develop in the water column caused by sulfidization of Fe-oxides and/or vivianite presumably governed by particle settling kinetics. After settling, the fate of the P-rich Fe-oxides and vivianite particles would be dictated by the prevailing conditions in the diagenetic environment. Under sulfate limited conditions P removed from the water column is likely to be retained in the sediment-pile, throttling productivity via a negative feedback (März et al., 2008b). When sulfate is available, however, reductive dissolution of Fe-oxides will liberate phosphate to the pore water which may be lost or retained dependent on the locus of dissolution and the availability of other important dissolved species (Ca^{2+}, Fe^{2+}, Mg^{2+}, F^-) and reductants (e.g., organic matter, CH_4).

Applying these principles to our understanding of Earth History is somewhat speculative but nonetheless interesting, with broad implications for P-cycling. In the largely low-sulfate ferruginous oceans prior to the GOE, the development of euxinia would have been scarce, enhancing phosphate shuttling to the sediment. If this phosphate was efficiently retained on a global-scale, then phosphate availability in these ancient oceans would have been low, especially considering the reduction in oxidative weathering (Reinhard et al., 2017). By contrast, throughout Earth's history euxinic marine environments have become more prevalent—a consequence of rising sulfate concentrations (Poulton, 2017). As discussed, euxinic conditions promote P recycling and its return to the water column; whereas P is more recalcitrant in ferruginous environments. In a simple sense, therefore, euxinic conditions are touted to be quasi self-sustaining (via a productivity feedback) whereas ferruginous conditions are not. In a wider Earth System sense, however, these gross generalizations may not be valid, and warrant further investigation. Sustained euxinia, for example, could lower sulfate inventories favoring the development of ferruginous conditions if S/Fe_{HR} ratios drop below 1.8 (e.g., Poulton and Canfield., 2011). Furthermore, unless reactive iron enrichments are solely derived from hydrothermal emanations, simple mass balance constraints dictate that sedimentary iron enrichments are unlikely to occur throughout an anoxic ocean and the source region must be depleted in reactive iron (e.g., Poulton and Canfield., 2011). Consequently, to understand the global effects of oxygen deficiency on P-cycling we must more completely understand the local controls on P-cycling and how oxygen deficiency developed on an event-by-event basis to successfully integrate these processes in an Earth system model.

Reviewer 2: We would like to express our gratitude to R2. Most of the points raised here were also raised by R1, we have attempted to cross reference between our responses to prevent repetition. We reply to each of the reviewer's comments in turn and have amended the manuscript as necessary.

R2.1). Comment: Although the chemical composition of the pore-water (pH, PO_4^{3-}, Ca^{2+} etc.) is lacking, a simple geochemical calculation on what kind of minerals (FeS, CFA, $Mg_3(PO_4)_2$, $Fe_3(PO_4)_2$) are expected to be precipitated in/above/under SMTZ would make the P-cycle in methane-rich environments clearer.

Reply: Pore water chemistry is essential to conduct a comprehensive series of calculations on mineral precipitation in marine sediments. As discussed in R1.1, we lack robust pore water data and thus we draw on PHREEQC calculations of pore water saturation indexes from other sites (Egger et al., 2015a, Baltic Sea, Fig. S8; März et al., 2018, open marine margins) to address this comment.

Hydroxyapatite saturation indexes above 0 suggest that the steady supply of phosphate from reductive dissolution of Fe-oxides creates thermodynamically favorable conditions for carbonate fluorapatite (CFA) precipitation around the SMTZ, whereas CFA formation appears to be a minor sink for pore water phosphate below the SMTZ (März et al., 2018). Higher saturation indexes for vivianite are typically obtained below the SMTZ. Here, the upward flux of Fe^{2+} from iron reduction and downward flux of phosphate from the reductive dissolution of Fe-oxides create favorable geochemical conditions for vivianite precipitation below the SMTZ, consistent with the vivianite distribution observed at Site 973-4. The solubility product constant K_{sp} of Mg phosphate is 10^{-24}, while the K_{sp} of vivianite is 10^{-36} (Nriagu, 1972), making the former mineral more soluble. Moreover, Mg concentrations are only about three orders of magnitude higher than those of Fe in marine sediments (e.g. Hu et al., 2015, Site D-5). Consequently, Mg phosphate precipitation is unlikely. Rather, Mg^{2+} is more likely to be co-precipitated with vivianite, forming Mg-rich vivianite below the SMTZ. This is clarified on line 18–21, page 11 and the following paragraph.

Besides phosphate minerals, Fe sulfides are enriched in and above the SMTZ. Pyrite is a common mineral in marine sediments where dissolved sulfide, produced by either organoclastic sulfate reduction (above the SMTZ) or sulfate driven anaerobic oxidation of methane (within the SMTZ), is trapped by Fe-oxides, forming Fe monosulfide. Fe monosulfides are gradually converted to pyrite as a permanent sink for sulfur. The acid volatile sulfur peak at ~900 cm depth contains large amounts of Fe monosulfides, and is referred to as the sulfidization front (S-front). The dissolved Fe is sourced either from the reductive dissolution of Fe-oxides by sulfide at the same depth or iron reduction at depth. Consequently, the formation of Fe sulfide is modulated by sulfate penetration depth. Clarifying text is found on line 17–19, page 8.

R2.2). Comment: Why is vivianite only observed/common under SMTZ (Fig 7a) instead of forming in/above SMTZ. What concentration of HPO_4^{2-} is expected when the Mg-rich vivianite is observed (Fig. 4) (The K_{sp} of $Mg_3(PO_4)_2$ are

three orders of magnitude higher than $Ca_3(PO_4)_2$, but the [Mg^{2+}] in pore-water are one order of magnitude higher than [Ca^{2+}]). Vivianite is lacking in ancient record. Would the vivianite formed here be converted to $Ca_3(PO_4)_2$ or what conditions are necessary for vivianite preservation in the sedimentary record to serve as a proxy for methane rich environment or Fe-AOM activity? In Fig 6, vivianite is only observed at 747 cm? Why is there no vivianite below the 900 cm depth according to the XRF result? There is an inconsistency between vivianite content determined via XRF and handpicking.

Reply: We did not identify any macro-vivianite within or above the SMTZ. Generally, vivianite is unstable in the presence of sulfide that is produced by sulfate reduction in/above the SMTZ, and is readily converted to pyrite (Berner, 1981). Previous studies suggest that phosphate concentrations are higher than ~100 µM in the SMTZ when potential vivianite is observed, so that enhanced phosphate flux could create favorable geochemical conditions for vivianite precipitation below the SMTZ (e.g. Egger et al., 2015; März et al., 2008a, 2018). Dissolved Mg concentrations at a nearby site range from 48.4 to 37.7 mM, while dissolved Ca concentrations decrease linearly from the sediment surface to the SMTZ (12.5–2.5 mM) where most of the dissolved Ca is consumed (Ye et al., 2016; Site B). Empirically, Ca tends to be precipitated as CFA independently, while Mg tends to be co-precipitated with vivianite rather than forming Mg phosphate (see R2.1).

Vivianite is apparently lacking in deep-time records. Whether this is an artifact of inefficient surveys and/or non-diagnostic extraction protocols remains to be shown (see text in Section 5.4, page 14). Generally, authigenic Ca-P concentrations increase with burial depth, likely due to the transfer of P from more labile forms into authigenic apatite. This sink switching is considered to be the dominant process of apatite authigenesis in marine sediments worldwide (e.g. Ruttenberg and Berner, 1993; Slomp et al., 1996). Therefore, it is possible that vivianite formed at Site 973-4 is partly converted to authigenic apatite at depth. However, as we stressed in R1.8, the relationship between apatite and vivianite abundances is not straightforward and the details of vivianite preservation and potential transformation remain fundamental unanswered questions.

Finally, there is some element of misunderstanding concerning the origin of the questioned data. Figure 6 displays XRD data derived from handpicked Fe-rich silicates (the grey to green mineral aggregates), whereas the XRD-derived data sourced from handpicked vivianite aggregates is shown in Figure 5a. Vivianite aggregates are only identified below the SMTZ. The vivianite found in the aggregates of Fe-rich silicates at 747 cm depth is intriguing, however, it is not surprising that XRD reveals mineral phases that evade detection optically. As discussed in R1.6 (see from line 5–12 on page 10), we argue that SMTZ was once shallower and speculate that the vivianite observed at 747 cm was precipitated beneath the SMTZ when it was closer to the sediment water interface. The subsequent downward migration of SMTZ would then be expected to have converted most of the vivianite to iron sulfide erasing the shallow vivianite record.

Exactly why the vivianite at 747 cm survived sulfidization is uncertain, however, the textual association with Fe-silicates implies that these phases may have armored the vivianite, preventing conversion to sulfide.

R2.3). Comment: Another concern is the recognition of the current and previous SMTZs. Either porewater or sediment has its own validity in revealing the characteristics and mechanisms of seepage. For example, the geochemical data obtained from the solid fraction of sediments and from authigenic carbonates provide time-averaged information on biogeochemical processes on a timescale of years to centuries. Sediment pore waters and seep-dwelling fauna, on the other hand, provide information on much shorter timescales, spanning from days to months. This issue needs to be considered and discussed in discussion. One needs to mention the nature of the seeps. It is well known that seeps are heterogeneous both in time and space. I would find interesting that they describe in a few words the inherent nature of seeps in the introduction section and consequently highlight their findings in the discussion section. The shift of former and current SMTZ is exactly caused by the varying of flux of fluids.

Reply: We agree with R2, and reiterate that pore water and solid phase data resolve processes acting on different timescales (line 24–30, page 8). We have discussed this in R1.6. If we had reliable pore water sulfate and methane data, this would constrain the depth of current SMTZ, reflecting seep activity on a timescale of days to years. Solid phase imprints, such as those seen at ~6–9 m depth (Figs. 7–9), reflect sulfate driven AOM in a SMTZ that has been more-or-less static over decadal to millennial time-scales. Given the constant sedimentation rate at Site 973-4, the position of the SMTZ is controlled by flux of methane-rich fluids from depth. The long-term migration of SMTZ has altered the solid phase records and controlled the distribution of vivianite, creating the mineralogical and geochemical distribution profiles we observe today. This is clarified from line 21, page 9 to line 3 on the following page.

Vivianite formation in methane-rich deep-sea sediments from the South China Sea

Jiarui Liu[1], Gareth Izon[2], Jiasheng Wang[1], Gilad Antler[3,4,5], Zhou Wang[1], Jie Zhao[1], Matthias Egger[6]

[1] State Key Laboratory of Biogeology and Environment Geology, College of Marine Science and Technology, School of Earth Sciences, China University of Geosciences, Wuhan, 430074, China
[2] Department of Earth, Atmospheric and Planetary Sciences, Massachusetts Institute of Technology, Cambridge, MA, 02139, USA
[3] Department of Earth Sciences, University of Cambridge, Cambridge, CB2 3EQ, UK
[4] Department of Geological and Environmental Sciences, Ben-Gurion University of the Negev, Beersheba, 84105, Israel
[5] The Interuniversity Institute for Marine Sciences, Eilat, 88103, Israel
[6] The Ocean Cleanup Foundation, Rotterdam, 3014 JH, the Netherlands

Correspondence to: Jiasheng Wang (js-wang@cug.edu.cn)

Abstract. Phosphorus is often invoked as the ultimate limiting nutrient, modulating primary productivity on geological timescales. Consequently, along with nitrogen, phosphorus bioavailability exerts a fundamental control on organic carbon production, linking all the biogeochemical cycles across the Earth system. Unlike nitrogen that can be microbially fixed from an essentially infinite atmospheric reservoir, phosphorus availability is dictated by the interplay between its sources and sinks. While authigenic apatite formation has received considerable attention as the dominant sedimentary phosphorus sink, the quantitative importance of reduced iron-phosphate minerals, such as vivianite, has only recently been acknowledged and their importance remains under-explored. Combining microscopic and spectroscopic analyses of handpicked mineral aggregates with sediment geochemical profiles we characterize the distribution and mineralogy of iron-phosphate minerals present in methane-rich sediments recovered from the northern South China Sea. Here, we demonstrate that vivianite authigenesis is pervasive in the iron oxide-rich sediments below the sulfate-methane transition zone (SMTZ). We hypothesize that the downward migration of the SMTZ concentrated vivianite formation below the current SMTZ. Our observations support recent findings from non-steady state post-glacial sedimentary successions, suggesting that iron reduction below the SMTZ, probably driven by iron-mediated anaerobic oxidation of methane (Fe-AOM), is coupled to phosphorus cycling on a much greater spatial scale than previously assumed. Calculations reveal that vivianite acts as an important burial phase for both iron and phosphorus below the SMTZ, sequestering approximately half of the total reactive iron pool. By extension, sedimentary vivianite formation could serve as a mineralogical marker of Fe-AOM, signalling low-sulfate availability against methanogenic and ferruginous backdrop. Given that similar conditions were likely present throughout vast swathes of Earth history, it is possible that Fe-AOM and vivianite authigenesis may have modulated methane and phosphorus availability on the early Earth, as well as during later periods of expanded marine oxygen deficiency. A better understanding of vivianite authigenesis, therefore, is fundamental to test long-standing hypotheses linking climate, atmospheric chemistry and the evolution of the biosphere.

1 Introduction

Phosphorus (P) is an essential nutrient, and its availability limits primary production on both short and long timescales (Algeo and Ingall, 2007; Ruttenberg, 2014). Marine sediments are known to regulate water column P availability, either retaining or releasing P dependent on the prevailing redox conditions (Delaney, 1998; Slomp et al., 1996). Phosphate is predominantly found as HPO_4^{2-} in seawater (hereafter termed PO_4), which is captured and shuttled to the seabed in association with organic debris (organic P) or adsorbed onto iron (Fe)-(oxyhydr)oxides (hereafter termed Fe-oxide bound P). Through a combination of organic matter remineralization and reductive dissolution of Fe-oxides, PO_4 is released into the sediment pore water where precipitation of P-bearing minerals has the potential to sequester P over potentially geologically relevant timescales (Jensen et al., 1995; Ruttenberg and Berner, 1993; Sundby et al., 1992). Authigenic carbonate fluorapatite (CFA) is typically assumed to be the dominant sedimentary P mineral, accounting for around half of global marine P burial (Ruttenberg, 2014). Another potentially important group of P burial phases, that have only recently been recognized, are Fe(II)-phosphate minerals such as vivianite ($Fe_3(PO_4)_2 \cdot 8H_2O$). The global importance of these phosphates, however, remains under-constrained.

Vivianite authigenesis requires pore water with elevated ferrous iron (Fe^{2+}) and PO_4 concentrations. Low-sulfate lacustrine settings typically satisfy these criteria, and vivianite is commonly reported from freshwater sediments (e.g., Fagel et al., 2005; Rothe et al., 2014; Sapota et al., 2006). In more sulfate-rich settings, the presence of a sulfate-methane transition zone (SMTZ) has been shown to provide favorable conditions for vivianite authigenesis (Egger et al., 2015a, 2016; Hsu et al., 2014; März et al., 2008a, 2018; Slomp et al., 2013). The production of dissolved sulfide by sulfate-dependent anaerobic oxidation of methane (SO_4-AOM) in the SMTZ, and the associated conversion of Fe-oxides to Fe-sulfides, results in elevated pore water PO_4 concentrations around the SMTZ (März et al., 2008a). The subsequent downward diffusion of PO_4 into sulfide-depleted pore water below the SMTZ can then lead to the precipitation of vivianite, if sufficient reduced Fe is available at depth (e.g., Egger et al., 2015a; März et al., 2018).

Possible sources of Fe^{2+} below the SMTZ are organoclastic Fe reduction, abiotic reductive dissolution of ferric-phases by sulfide, anaerobic oxidation of methane coupled to the reduction of ferric Fe (Fe-AOM), as well as more cryptic and less well understood mechanisms (Egger et al., 2017 and references therein). Of these, Fe-AOM is often advocated as the most likely mechanism, supplying plentiful Fe^{2+} at the expense of methane due to the 8:1 stoichiometric conversion of Fe to methane (Eq. 1; Amos et al., 2012; Beal et al., 2009; Crowe et al., 2011; Egger et al., 2015b, 2016, 2017; Norði et al., 2013; Riedinger et al., 2014; Segarra et al., 2013; Sivan et al., 2011; Wankel et al., 2012).

$$CH_4 + 8Fe(OH)_3 + 15H^+ \rightarrow HCO_3^- + 8Fe^{2+} + 21H_2O \quad \text{(Eq.1)}$$

Iron-mediated AOM can be performed by anaerobic methane oxidizing archaea (ANME) who oxidize methane nonsyntropically, exploiting soluble and nanophase ferric iron (Fe^{3+}) as electron acceptors (Ettwig et al., 2016; Scheller et al., 2016). The presence of large multi-haem cytochromes (proteins that mediate electron transport) and type IV pili (cellular appendages) detected in the genomes of ANME hint that these archaea may also be able to exploit solid Fe-oxides via extracellular electron transport (McGlynn et al., 2015; Wegener et al., 2015). Moreover, the experimental approach of Bar-Or

et al. (2017) reveals that more refractory reactive Fe-oxides (e.g., magnetite and hematite) can also serve as electron acceptors for Fe-AOM. While biochemical investigations of *Methanoperedens ferrireducens* and *Methanosarcina activorans* have further illuminated the possible mechanistics of Fe-AOM (Cai et al., 2018; Yan et al., 2018), the modes and pathways of Fe-AOM remain enigmatic and warrant further exploration.

Vivianite authigenesis, potentially fueled by Fe-AOM, couples the biogeochemical cycles of Fe, P, sulfur (S) and carbon (C) in the deep biosphere. Given the importance of these elemental cycles within the Earth System, knowledge about vivianite precipitation and preservation in marine sediments is essential. While the database of vivianite occurrences in marine systems is growing, most of these records are from sites with atypical and time-variable stratigraphic records. For example, much of the work to-date has focused on vivianite authigenesis in non-steady state post-glacial sedimentary successions from marginal basins like the Baltic and Black Seas (Dijkstra et al., 2016, 2018a, 2018b; Egger et al., 2015a; Reed et al., 2016). In these settings, post-glacial sea-level rise resulted in the accumulation of organic rich sediments overlying organic-poor lacustrine deposits. Other reports of possible vivianite formation in marine systems are from deep-sea fan sediments (Burns, 1997; März et al., 2008a, 2018), as well as from accretionary wedge sediments (Hsu et al., 2014). Consequently, a more detailed understanding of vivianite authigenesis, and the interplay between CH_4, S, Fe and P in open marine sediments, will improve our ability to read ancient sedimentary records and to more adequately test hypotheses linking nutrient availability, climate and biospheric evolution.

In this study, we combine microscopic and spectroscopic analyses of handpicked mineral aggregates with bulk geochemical analyses to characterize the distribution and mineralogy of Fe-phosphate minerals in the methane-rich deep-sea sediments preserved in the Taixinan Basin, northern South China Sea (Fig. 1). X-ray diffraction and down core abundance records reveal vivianite authigenesis in this open marine sedimentary system. We further discuss the pathways for vivianite authigenesis below the SMTZ and the role of anaerobic methane oxidation. Our results support recent findings that vivianite formation can be an important burial mechanism for Fe and P in methane-rich marine sediments, indicating that vivianite authigenesis may have been more pervasive in the Earth's past.

2 Geological background and study site

The Taixinan (or Southwestern Taiwan) Basin is located east of the northern continental slope of the South China Sea (Fig. 1), separating a passive margin and an active accretionary wedge (Liu et al., 1997). As a Cenozoic hydrocarbon-bearing sedimentary basin featuring 1–4 km of sediment accumulation, the Taixinan Basin represents a promising area for gas hydrate and cold seep exploration (McDonnell et al., 2000). For example, a large seep-induced carbonate buildup (Jiulong Methane Reef, Site 1–3), covering about 430 km^2, was discovered during the R/V *SONNE* Cruise SO-177 in 2004 (Han et al., 2008; Suess et al., 2005). East of these inactive seeps, Site F on the Formosa Ridge represents one of the most vigorous cold seeps reported from within the South China Sea, supporting a large and diverse chemosynthetic ecosystem (Feng and Chen, 2015; Feng et al., 2015, 2018; Hsu et al., 2017). Moreover, massive gas hydrates were documented during China's second major gas

hydrate expedition (GMGS-2) in 2013 (Sha et al., 2015; Zhang et al., 2015b), which further confirms that gas hydrates are well developed in the Taixinan Basin. Accordingly, given that the position of the SMTZ is governed by the flux of methane-rich fluids from depth, such a methane-rich area provides an ideal natural laboratory to explore how millennial-scale variations in methane flux influence vivianite distribution in continental margin settings.

This contribution exploits a piston core (total length of 13.85 m) that was taken at Site 973-4 (118°49' E, 21°54' N) in 2011 during a cruise with R/V *Ocean VI* (Fig. 1). Retrieved from the lower continental slope at a water depth of 1666 m, core 973-4 is dominated by dark-green silty clay. The only deviation in grain-size is a siltier layer between 455−605 cm depth, whose coarse fraction (> 65 μm) increases in association with increased abundances of foraminifera and Fe-rich silicates (Fig. 2a). Radiocarbon- and $\delta^{18}O$-derived age models (Fig. 2a) suggest sedimentation rates were relatively constant (32 cm ka^{-1}) throughout the ~40-thousand-years (ka) of deposition encompassed by core 973-4. Again, the only departure is associated with the coarser layer deposited during the Last Glacial Maximum, which yields atypically old radiocarbon ages relative to the surrounding sediment. These observations are consistent with increased slumping and/or turbidity currents (e.g., Zhong et al., 2015) driven by gas hydrate destabilization on the upper continental slope, and concomitant continental-slope failure during sea-level low stands (Kennett et al., 2003; Maslin et al., 2004).

3. Methods

After retrieval, core 973-4 was cut into sections and stored below 4 °C. These core sections were then split, subsampled and frozen (−20 °C) immediately after the cruise. Frozen samples were divided into two subsamples: the first subsample was used to isolate specific mineral phases via conventional handpicking (e.g., Lin et al., 2016a) and the second was homogenized for chemical analyses. All sample powders were kept frozen to minimize oxidation.

After drying at 60 °C for 24 h, the first set of subsamples were sieved with distilled water allowing the coarse fraction (> 65 μm) to be collected. Mineral aggregates were then identified and handpicked from the greater than 65 μm fraction (coarse component) under a stereomicroscope. The weight of these mineral fractions, along with the total coarse component, were determined and their concentrations were expressed relative to the initial dry mass of the sample. The morphology and chemical composition of the handpicked minerals were investigated using a FEI Quanta 450 FEG scanning electron microscope (SEM) in energy dispersive spectroscopy (EDS) mode. Power X-ray diffraction (XRD) analysis of the handpicked samples was performed using Ni-filtered Cu Kα radiation on a Panalytical X'Pert Pro diffractometer. The X-ray diffractometer was operated at 40 kV and 40 mA over a 3–65° 2θ range. The analytical step size was 0.017° with a measurement dwell time of 0.4 s per step. Raman analysis of the handpicked samples was performed by a JY/Horiba LabRam HR Raman system, using 532.06 nm (frequency doubled Nd:YAG) laser excitation, a 50× Olympus objective, and a 300-groove/mm grating.

Two different operationally defined solid-phase Fe pools were determined chemically exploiting separate aliquots of freeze-dried sample (e.g., Holmkvist et al., 2011, 2014). Briefly, the most readily acid-soluble Fe phases, including amorphous Fe (hydro)oxides and ferrihydrite (Haese et al., 1997; Wallmann et al., 1993), were extracted via agitation with an anoxic 0.5 M

HCl solution for one hour. The Fe(II) content of this extract was then determined via the 1, 10-phenanthroline method (Amonette and Templeton, 1998), followed by the total Fe content (i.e., Fe(II) + Fe(III)) with a 1, 10-phenanthroline and 1% (w/v) hydroxylamine hydrochloride assay. The poorly crystalline Fe(III) (oxy)hydroxide content was then calculated as the difference between the reduced and mixed-valence Fe determinations. More crystalline Fe-oxides, including goethite, hematite and part of the poorly reactive sheet silicate Fe fraction, were then quantified after treating a separate sample aliquot with a mixed dithionite-citrate-acetic acid solution for two hours (Poulton and Canfield, 2005). The Fe(III) and manganese (Mn) contents of the resulting supernatants were measured by atomic absorption spectrometry (Pgeneral, TAS-990). Replicate analysis of samples and standards (CUG-2 and CUG-3, Zhang et al., 2018d) displayed relative standard deviations (RSD) of better than 5%. Compared to the more well-documented dithionite method, the HCl method has not been as well calibrated. Therefore, for the ensuing discussion, we refer to dithionite-extractable Fe and Mn as reactive Fe-oxides and reactive Mn, respectively.

Pore water samples from Site 973-4 were not immediately extracted; instead, they were obtained several months later via centrifugation of previously frozen subsamples (Zhang et al., 2014). Consequently, we believe that the pore water chemistry of Site 973-4 may have been compromised, and is more likely to reflect post-recovery oxidation and/or contamination rather than in-situ sediment processes (Fig. 2b). Fortunately, pore water sulfate and methane concentrations are better constrained at several surrounding sites (Site DH-CL11, Site B and Site HD319), which are separated from Site 973-4 by less than a few kilometers (Lin et al., 2017b; Lu et al., 2012; Ye et al., 2016). Like Site 973-4, the adjacent sites are lithologically similar and dominated by silty clay. Moreover, the pore water chemistry from the surrounding sites is broadly analogous (Fig. 2b), indicating that each site was likely subject to the same depositional process(es). Consequently, in the absence of robust pore water data, we synthesize observations from these neighboring sites to estimate the position of the SMTZ at Site 973-4. We stress that we do not advocate this approach to replace pore water analysis but, in its absence, we argue that pore water data from nearby sites, when combined with solid-phase distributions from Site 973-4, allow us to estimate the approximate position of the SMTZ, albeit with caveats. Pore water extraction from Site DH-CL11 was conducted on shore via centrifugation, exploiting sample aliquots that had been immediately taken and stored under vacuum at −80 °C (Lin et al., 2017). Pore water samples from Site B and Site HD319 were collected immediately after recovery by vacuum extraction (Lu et al., 2012; Ye et al., 2016). At each site, the pore water sulfate contents were determined by ion chromatography; whereas, pore water methane concentrations were determined via sediment plug sampling and gas chromatographic analysis of the resultant headspace gas (Lin et al., 2017; Lu et al., 2012; Ye et al., 2016). The pore water chemistry of these adjoining sites reveals consistently shallow SMTZs, found between ~700 and 880 cm depth, which, via extension, is where we tentatively place the present-day SMTZ at Site 973-4.

Previously published data was determined using separate aliquots of the same subsamples exploited herein. This earlier work followed established protocols and full methodological details are provided in the respective papers. Accordingly, only a brief description is provided here: Acid volatile sulfide was liberated via HCl distillation and trapped by zinc acetate, its concentration was then determined spectrophotometrically (Zhang et al., 2014). Pyrite aggregates were handpicked from, and

expressed relative to, the coarse-fraction (> 65 μm). The sulfur isotopic composition of handpicked pyrite was determined directly via flash combustion using a Delta V Plus isotope ratio mass spectrometer (IRMS) interfaced with a Flash elemental analyzer (Lin et al., 2015). The solid-phase distribution of P was revealed through the SEDEX sequential extraction scheme (Ruttenberg, 1992). Iron-bound P and authigenic carbonate fluorapatite were extracted by citrate-bicarbonate-dithionite and Na-acetate buffer, respectively (Zhang et al., 2018b). The carbon isotopic composition of total inorganic carbon was determined using a Finnigan MAT-252 IRMS after initial treatment with phosphoric acid (Ou, 2013; Zhang et al., 2018c). Finally, magnetic susceptibility data was generated using a MFK1-FA kappameter (Lin et al., 2017a).

4. Results

4.1 Morphology and chemical composition of mineral aggregates

Two types of dark mineral aggregates were identified. Examination of these handpicked mineral aggregates under a stereomicroscope revealed that the opaque blue to black crystals (0.1–1 μm diameter) were only present in samples below ~920 cm sediment depth (Fig. 3a). By contrast, stereomicroscope and SEM observations showed that pyrite is pervasive throughout the upper part of the core, observed in samples at ~310–880 cm depth. Moreover, SEM observations of the blue to black mineral phase found below the SMTZ disclosed a distinctive morphology, displaying spherical aggregates of radiating lath-, platy- and needle-shaped crystals (Figs. 3b−e, g). This distinct morphology strongly resembles vivianite crystals identified from the Baltic Sea (Dijkstra et al., 2016; Egger et al., 2015a) and lacustrine sediments (Rothe et al., 2014, 2015). Major peaks of O, Fe, P were observed in the EDS spectra of the blue to black aggregates (Fig. 3f), constituting 39%, 28%, and 19% of the aggregates by mass (n=12), respectively. The O, Fe, P mass-ratios and the molar Fe/P ratio (0.83) from EDS analyses also approximate those reported from sedimentary vivianite from the Bothnian Sea (0.82 and 0.86), as well as synthesized vivianite (0.99; Egger et al., 2015a). Additional minor peaks of Mg, Si, Al, Ca, Mn, S were also observed in the EDS spectra, constituting 4.9%, 1.8%, 1.6%, 1.6%, 1.2%, 1.2% of the aggregates by mass (n=12), respectively. The Fe–Mg–Mn ternary plot of these aggregates (Fig. 4) reveals that the Fe/(Fe+Mg) ratios range from ~0.64 to 0.98, while the Mn/(Mn+Fe) ratios range from ~0 to 0.05. These observations are similar to the high-Mg, low-Mn vivianite identified in the sediments recovered from offshore southwestern Taiwan (Hsu et al., 2014).

Additional grey to green mineral aggregates were observed in samples throughout the sediment core. These particles feature smooth surfaces (Fig. 3h), while their EDS spectra show high intensity Fe, Si, O peaks (Fig. 3i), suggesting an Fe-rich silicate phase.

4.2 XRD and Raman analyses of mineral aggregates

X-ray diffraction analyses confirm that the blue to black mineral aggregates found below the SMTZ are vivianite nodules (Fig. 5a). The high intensity narrow peak observed at 13.2° typifies XRD spectra obtained from both natural and synthetic vivianite crystals (Dijkstra et al., 2016; Egger et al., 2015a; Grizelj et al., 2017; Rothe et al., 2014). Other Mg- or Fe-bearing phosphate

minerals such as metavivianite were not recognized in diffractograms of our samples. Raman analyses showed a curved baseline with broad peaks (Fig. 5c), potentially caused by fluorescence interference from the samples (Kagan and McCreery, 1994). Despite these limitations, some peaks can still be recognized, especially the peak around 1000 cm^{-1}. These spectral features are also consistent with the Raman spectra of vivianite crystals (Piriou and Poullen, 1984), and thus offer an additional line of evidence supporting the results obtained from SEM-EDS and XRD analyses.

The grey to green mineral aggregates are mainly composed of chlorite, illite, quartz, and albite. Additional peaks including orthoclase, siderite, calcite, dolomite, pyrite and vivianite were also identified (Figs. 5b and 6). The XRD spectra indicated that some illite peaks might belong to mixed-layer illite/smectite. Glauconite is a green Fe-rich member of illite group and is an abundant authigenic mineral at water depths between 30 and 2000 m (Porrenga, 1967). Considering its EDS spectra, with high intensity Fe, Si, O peaks, it is likely that the illite-group minerals identified in core 973-4 may include a considerable glauconite component. Besides Fe-rich illite, or possibly even glauconite, chlorite is another Fe-rich sheet silicate that would also give similar EDS spectra. Given the difficulties in distinguishing between low abundance Fe-rich clays in complex marine sediments by XRD, the grey to green mineral aggregates are simply referred to as Fe-rich silicates from here on.

4.3 Down-core variations of mineral aggregates

The distribution of authigenic minerals at Site 973-4 displays distinct down-core variability, especially at and around the SMTZ. Substantial coarse grained pyrite was observed between ~560–880 cm depth with a peak around the SMTZ. Handpicked vivianite aggregates were only identified between ~920–1370 cm depth in the sediment (Fig. 7a). The concentration of vivianite ranges from 0.02 wt.‰ to 1.58 wt.‰ directly below the SMTZ (920–1175 cm depth), decreasing to lower values (0 to 0.36 wt.‰) towards the base of the core (1175–1370 cm depth). Dark laminations and reddish-brown nodules are prominent between 892–904 cm depth where acid volatile sulfur (AVS) displays a sharp peak at the base of the SMTZ (Fig. 9b). Major peaks of O and Fe were observed in the EDS spectra of these nodules, while lower intensity S peaks were only observed in a few samples. Nodules of AVS usually turn reddish-brown during post-sampling oxidation, thus most of the nodules found at the base of the SMTZ are most likely oxidation products of AVS.

Fe-rich silicates were distributed throughout the core (Fig. 7b), displaying a peak between 455–605 cm depth. This layer has an elevated coarse-grained component and is associated with atypically old radiocarbon ages (Fig. 2a). The XRD spectra reveal that the Fe-rich silicates within this layer include more chlorite, differing from the composition of background Fe-rich silicates (Fig. 6). Compared with the high abundances of Fe-rich silicates observed above (8.48 wt.%) and below (2.94 wt.%) the SMTZ, the abundance of Fe-rich silicates within the SMTZ is servilely diminished, ranging from 0.01 wt.% to 0.16 wt.%.

4.4 Solid phase iron and manganese geochemistry

Ferric iron minerals were quantified using two different extraction methods, with both approaches yielding broadly consistent trends (Fig. 8a). The absolute concentrations of Fe (oxy)hydroxides and reactive Fe-oxides are low immediately above and within the SMTZ, reaching a minimum of 34 µmol g^{-1} and 76 µmol g^{-1} within the more silty layer, respectively. Their respective

concentrations increase to 173 µmol g^{-1} and 238 µmol g^{-1} at 900 cm depth and remain high around 123–161 µmol g^{-1} and 174–235 µmol g^{-1} below the SMTZ (Fig. 8a). Since more crystalline Fe minerals (e.g. goethite, hematite) are extracted by the dithionite-citrate-acetic acid solution (Poulton and Canfield, 2005; Raiswell et al., 1994), the concentration of reactive Fe-oxides is higher than that of Fe (oxy)hydroxides throughout the core. Therefore, for simplicity, reactive Fe-oxides will be referred to as Fe-oxides in the following discussion. Reactive Mn concentrations range from 1.6 µmol g^{-1} to 4.6 µmol g^{-1}, which is nearly two orders of magnitude higher than those of Fe (oxy)hydroxides and reactive Fe-oxides. Fe and Mn show similar distribution patterns with depth (Fig. 8). Since AVS oxidizes to dithionite and oxalate extractable Fe phases during freeze-drying or exposure to air (Canfield, 1989; Morse, 1994), the obvious peak of Fe-oxides at ~900 cm depth (Fig. 8a) is partly attributed to AVS oxidation during sample storage and treatment.

5. Discussion

5.1 The role of the SMTZ in marine vivianite authigenesis

Vivianite precipitation is favored in anoxic and non-sulfidic settings; conditions that are frequently encountered in lacustrine sediments (Berner, 1981; Nriagu, 1972; Rothe et al., 2016). Recently, the presence of a SMTZ has been shown to play a principle role in vivianite formation, extending the importance of vivianite authigenesis to marine settings where sulfate is more readily available (Egger et al., 2015a; Hsu et al., 2014; März et al., 2008a; Slomp et al., 2013). Within the SMTZ, sulfate-driven AOM consumes sulfate and methane whilst liberating sulfide and bicarbonate. The resultant sulfide is rapidly fixed, initially as Fe monosulfides and ultimately, under an excess of sulfide, as pyrite, acting as a permanent sink for sulfur. Therefore, given a constant methane flux, the locus of Fe sulfide precipitation is governed by the depth to which sulfate penetrates the sediment pile. Pyrite formation within the SMTZ is characterized by a strong ^{34}S enrichment along with characteristic overgrowth textures (Borowski et al., 2013; Jørgensen et al., 2004; Lin et al., 2016a; Lin et al., 2016b). In addition, sulfate driven AOM enriches authigenic carbonates in ^{12}C, as they inherit their carbon isotopic signature from ^{13}C-depleted methane (Peckmann and Thiel, 2004; Treude et al., 2005). At Site 973-4, between ~560 and 880 cm depth, the pyrites display a pronounced increase in $\delta^{34}S$ values in concert with an excursion to low $\delta^{13}C$ values registered in the total inorganic carbon pool (Fig. 9). The ingrowth of these distinctive isotopic signatures within the solid-phase record at Site 973-4 requires that the SMTZ has remained stable between 560–880 cm depth for millennia (März et al., 2008a). Caused by the conversion of Fe-oxides to pyrite, the drop in magnetic susceptibility at the same depths (Fig. 8b) provides support for this inference. In detail, however, precisely constraining the depth of the current SMTZ at Site 973-4 is more difficult, complicated by the lag-time of the solid-phase record and the absence of reliable pore water data (discussed below). Nevertheless, complications aside, the SMTZ depth-estimate derived from Site 973-4's solid-phase record is broadly consistent with that inferred from neighboring pore water profiles (Fig. 2b).

Reactive Fe-oxides and Fe-rich silicates are gradually consumed within the SMTZ via reductive dissolution by sulfide and subsequent conversion to pyrite (Figs. 7b and 8a). Consequently, any excess sulfide descending from the SMTZ is trapped as

Fe monosulfides upon reaction with more readily available Fe-oxides at depth. This reaction zone, often referred to as the sulfidization front (S-front), is a common feature in Fe-rich marine sediments (Egger et al., 2016; Holmkvist et al., 2014; Jørgensen et al., 2004; Riedinger et al., 2017) and is recorded at Site 973-4 as a pronounced AVS peak at ~900cm depth (Fig. 9b). Besides liberating Fe, and 'seeding' Fe-sulfides, reductive dissolution of Fe-oxides by sulfide also releases a significant amount of Fe-oxide bound P into the pore water around the SMTZ (Egger et al., 2015a; März et al., 2008a; Schulz et al., 1994; Slomp et al., 2013). Previous studies have demonstrated that PO_4 concentrations typically exceed ~100 µM in the SMTZ when vivianite is observed, providing empirical evidence for a SMTZ-derived P source for subsurface vivianite precipitation (e.g. Egger et al., 2015; März et al., 2008a, 2018). Unfortunately, there is no reliable PO_4 pore water profile from Site 973-4; however, the conversion of Fe-oxides to pyrite and the associated release of Fe-oxide bound P to the pore water should also be documented within the solid-phase records (Egger et al., 2015a, 2016). Consequently, the distinct minimum of Fe-bound P around the SMTZ, and a sharp peak directly below the SMTZ, strongly suggests that sink-switching from Fe-oxide bound P to reduced Fe-phosphates is occurring at Site 973-4 (Fig. 9b).

X-ray diffraction analyses show that the blue to black aggregates found exclusively below the inferred position of the SMTZ are vivianite aggregates (Fig. 5a). Other Mg- or Fe-bearing phosphate minerals such as metavivianite were absent from the XRD spectra, advocating that the Fe-P-O aggregates identified by SEM-EDS and Raman are indeed vivianite (Figs. 3 and 5). The restriction of vivianite nodules to below the SMTZ strongly supports the SMTZ-catalyzed model of vivianite authigenesis resulting from inferences gleaned from the juxtaposition of lacustrine and post-glacial marine sediments (Egger et al., 2015a, 2016; Slomp et al., 2013). Furthermore, the broad peak in Fe-bound P above the SMTZ likely reflects retention and re-adsorption of ascending PO_4 to shallower Fe-oxides (Fig. 9b), as suggested previously based on observations from the Zambezi deep-sea fan (März et al., 2008a).

Accepting the uncertainties and extending the pore water chemistries from adjacent sites to Site 973-4, suggests that the SMTZ currently resides around 700–880 cm depth (Fig. 2b), deeper than one would predict based on the solid-phase records alone. This discrepancy is most likely due to the different response times of the aqueous- and solid-phase records, implying that the SMTZ has not been stationary over the cored interval. We reconcile the preservation of Fe-oxides and the absence of pyrite below the SMTZ with a rapid ascent of the SMTZ. Such a rapid shallowing of the SMTZ would limit sulfide exposure, causing incomplete reduction and sulfidization of the deeper reactive Fe pool (März et al., 2018). Following its hypothetical ascent, the SMTZ must have then remained stable between 560–880 cm, leaving pronounced imprints within the pyrite, Fe-oxide, Fe-silicate, total inorganic carbon and magnetic susceptibility profiles (Figs. 7–9). Assimilating these observations, we suggest that the SMTZ descended from ~560–700 cm to its current position at ~700–880 cm depth. Given that the sedimentation rate at Site 973-4 was almost constant over the duration of the core (Fig. 2a), we attribute the hypothesized downward migration of the SMTZ to a change in the methane flux. Furthermore, we suggest that the evolution of the SMTZ reflects glacial–interglacial sea-level changes, with the sea-level low stand at Last Glacial Maximum decreasing hydrostatic pressures, destabilizing methane clathrates (Kvenvolden, 1993) and promoting a rapid upward migration of the SMTZ due to enhanced methane fluxes (Borowski et al., 1996). Conversely, the subsequent Holocene sea-level rise would have diminished methane

fluxes, instigating a slow downward migration of the SMTZ to its current position. These observations advocate that hydrate-derived methane fluxes are heterogeneous and, along with vivianite authigenesis, are likely to have been variable on millennial time-scales (Ruppel and Kessler, 2017; März et al., 2018).

Vivianite is reactive toward sulfide and, hence, would be readily converted to Fe-sulfide phases under H_2S-rich conditions (Berner, 1981). Therefore, when the SMTZ was shallower, we propose that vivianite was precipitated above where it is currently observed and has subsequently been dissolved. Tentative evidence for diagenetic modification of the original vivianite distribution is seen in our XRD data. Here, XRD analysis indicates the presence of vivianite within the current SMTZ at 747 cm depth, yet handpicking failed to identify any coarse vivianite (Figs. 6–7a). Dissolution of freshly precipitated vivianite should be promoted by the downward migration of the SMTZ and increased environmental sulfide availability, concentrating vivianite below the SMTZ and producing the observed stratigraphic distribution (Fig. 7a). Exactly why the vivianite at 747 cm depth survived sulfidization remains uncertain, however, the textual association with Fe-silicates implies that these phases may have armored the vivianite, preventing its conversion. In the event of the SMTZ shallowing, any sub-SMTZ vivianite could potentially be preserved providing the environment remained H_2S-free and no other mineral transformations occurred (see below). Thus, we hypothesize that long-term migration patterns of the SMTZ will alter the solid-phase record and control the distribution of vivianite. The integrative effect, of course, creates the mineralogical and geochemical distribution profiles we observe today.

5.2 The importance of anaerobic oxidation of methane in vivianite authigenesis

The ubiquity of vivianite aggregates below the SMTZ at Site 973-4 requires that there is a deep source of Fe^{2+}. Recent field and laboratory studies have suggested that anaerobic oxidation of methane can be coupled to the reduction of Fe-oxides (Beal et al., 2009; Egger et al., 2015b, 2016, 2017; Riedinger et al., 2014; Sivan et al., 2011). Specifically, it has been suggested that insoluble Fe-oxides can be exploited by solitary anaerobic methanotrophic archaea (ANME) as electron acceptors, facilitating methane oxidation via extracellular electron transfer (McGlynn et al., 2015; Rotaru and Thamdrup, 2016; Scheller et al., 2016; Wegener et al., 2015). Moreover, sediment incubation experiments demonstrate that more poorly reactive Fe minerals (e.g., magnetite and hematite) are also bioavailable and, therefore, could potentially fuel Fe-AOM (Bar-Or et al., 2017). Extending these in vitro observations to natural settings suggests that bioavailable Fe-oxides, and potentially reactive Fe-rich silicates below the SMTZ may be available for bacterial Fe reduction coupled to methane oxidation. Considering the 8:1 Fe-CH_4 stoichiometry (Eq. 1; Beal et al., 2009), Fe-AOM certainly has the potential to yield significant quantities of Fe^{2+}. In general, large amounts of dissolved PO_4 are released into the pore water by sulfate-driven AOM within the SMTZ (e.g., März et al., 2008a), while bacterial Fe reduction using Fe-oxides below the SMTZ triggers the release of both Fe^{2+} and PO_4 (Egger et al., 2015a). Supported by abundant Fe-oxides and Fe-silicates below the SMTZ, bacterial Fe reduction, probably driven by methane oxidation, promotes vivianite authigenesis, exchanging P originally associated with Fe-oxides to vivianite-housed P (Fig. 10). As a byproduct, Fe-AOM is known to produce alkalinity (Beal et al., 2009), which can stabilize vivianite by raising the pH values of the pore water to between 6 and 9 (Rothe et al., 2016).

Besides Fe-AOM, other potential sources of Fe^{2+} below the SMTZ include organoclastic Fe reduction (Lovley, 1997; Severmann et al., 2006) and abiotic reductive dissolution by sulfide (Canfield et al., 1992; Poulton et al., 2004). A pronounced AVS peak at ~900 cm depth constrains the depth of the sulfidization front at Site 973-4 (Fig. 9b). In similar systems, dissolved sulfide is limited below the S-front (Egger et al., 2016; Jørgensen et al., 2004; Riedinger et al., 2017). As vivianite is unstable in the presence of sulfide (Dijkstra et al., 2018a), its presence below ~920 cm depth supports the absence of appreciable amounts of dissolved sulfide. Additionally, extremely elevated concentrations of Fe^{2+} are frequently observed below the S-front (Egger et al., 2016; Holmkvist et al., 2011, 2014; Jørgensen et al., 2004; Treude et al., 2014). Given the reactivity of Fe^{2+} toward sulfide, the existence of the latter would rapidly titrate the former, forming Fe monosulfides rather than reacting with Fe-oxides (Berner, 1967). We therefore conclude that abiotic sulfide-mediated reductive dissolution of Fe-oxides is unlikely to provide significant amounts of Fe^{2+} below the SMTZ.

Although unequivocally precluding organoclastic Fe reduction below the SMTZ remains difficult, the total organic carbon content throughout core 973-4 is low and more-or-less invariant, with an average value of 0.72 ± 0.19 wt.% (Zhang et al., 2014). These relatively low concentrations of likely reworked organic matter may be insufficient to fuel organoclastic Fe reduction (Riedinger et al., 2014). Consequently, the importance of organoclastic Fe reduction is likely to be limited by the quality and quantity of organic matter burial below the SMTZ (Egger et al., 2017; Riedinger et al., 2014; Sivan et al., 2011).

Besides its major constituents (Fe, O and P), sedimentary vivianite aggregates are usually enriched in other minor elements, such as Mg (Burns, 1997; Dijkstra et al., 2018b; Hsu et al., 2014) or Mn (Dijkstra et al., 2018b; Egger et al., 2015a; Fagel et al., 2005; Nakano, 1992; Sapota et al., 2006). The solubility product constant K_{sp} of Mg phosphate is 10^{-24}, while the K_{sp} of vivianite is 10^{-36} (Nriagu, 1972), making the former mineral more soluble. Moreover, Mg concentrations are only about three orders of magnitude higher than those of Fe in marine sediments (e.g. Hu et al., 2015). Therefore, Mg phosphate precipitation is unlikely and Mg^{2+} is more likely to be co-precipitated with vivianite below the SMTZ. In the absence of appropriate pore water data, we rely on datasets from a proximal site that reveals high concentrations of dissolved Mg (48.7–53.0 mM) but low concentrations of dissolved Mn (0.4–5.1 µM; Site D-5, Hu et al., 2015). These pore water chemistries are reflected in the elemental composition of the vivianite isolated from core 973-4 (Fig. 4). Manganese displays similar geochemical properties as Fe, yet it has been shown to be a substantially more energetically favorable electron acceptor during organic matter or methane oxidation (Beal et al., 2009). We reconcile the extremely low vivianite-housed Mn contents at Site 973-4 with the generally low sedimentary Mn abundances (Fig. 8b), concluding that Mn-mediated AOM was probably of limited importance Site 973-4. Taken together, while we cannot completely exclude organoclastic Fe reduction as a potential source of Fe^{2+}, along with observations of others, we use the discussed stratigraphic distribution of various sedimentary mineral phases to argue that Fe-AOM is the most likely deep source of Fe^{2+} necessary to promote vivianite authigenesis observed below the SMTZ. Consequently, we speculate that where basal waters are oxygenated, sedimentary vivianite formation could serve as a mineralogical marker of Fe-AOM, signalling low-sulfate availability against methanogenic and ferruginous backdrop.

Important P and Fe phases that could compete with vivianite formation are authigenic apatite and Fe monosulfides. PHREEQC calculations of pore water saturation indexes (Egger et al., 2015a; März et al., 2018) show that hydroxyapatite saturation

indexes (SI) typically reach a maximum (above 0) around the SMTZ but drop to background values below the SMTZ, suggesting that the steady supply of PO_4 from reductive dissolution of Fe-oxides fosters thermodynamically favorable conditions for apatite authigenesis in proximity to the SMTZ. While there are no reliable pore water data from Site 973-4, dissolved Ca^{2+} concentrations from Site B are consistent with ongoing apatite authigenesis, with a linear down-core decrease from the sediment-water interface to the upper part of the SMTZ (12.5–2.5 mM) where most of the Ca^{2+} has been consumed (Ye et al., 2016). To our knowledge, however, there are no available dissolved F^- and PO_4 data to unequivocally confirm apatite precipitation rather than other calcium-harboring phases. Higher SI for vivianite are generally obtained below the SMTZ, consistent with the vivianite distribution observed at Site 973-4. Importantly, vivianite authigenesis occurs below the sulfidization front (~900 cm) implying that FeS precipitation is kinetically favored over vivianite precipitation. We speculate, therefore, that the pore water chemistry and the activity of sulfidization front will influence the depth of vivianite formation. Intensified activity at the sulfidization front would liberate more PO_4. The concomitant sulfide flux, however, may serve to nullify the ascent of Fe^{2+} from depth, especially as highly reactive Fe is consumed, preventing vivianite formation or, more likely, confining its authigenesis to deeper into the sediment pile. Unfortunately, we do not have the data to definitively test the hypothesized competing role between apatite, FeS and vivianite authigenesis. Nevertheless, any process that serves to deplete pore water PO_4 and Fe^{2+} will hypothetically compete with vivianite formation. Future work should focus on generating comprehensive pore water and solid phase data sets, which when coupled with reactive transport models, will better link the rate of sulfide production in the SMTZ, the amount of reactive Fe-oxides and the generation potential of different authigenic P phases below the SMTZ.

5.3 Quantifying the importance of vivianite as sedimentary sinks of iron and phosphorus

Sequential P extractions (SEDEX; Ruttenberg, 1992), conducted by Zhang et al. (2018b), demonstrate that authigenic carbonate fluorapatite (Ca-P, Fig. 9c) accounts for up to 55% of the total P (702 μmol g^{-1}) buried at Site 973-4. Fe-bound P is generally lower than authigenic Ca–P, accounting for 27% and 13% of the total P burial above (613 μmol g^{-1}) and below the SMTZ (844 μmol g^{-1}), respectively. These results emphasize the role of Fe-bound P as an important mechanism for P burial in continental margin settings (Slomp et al., 1996). Interestingly, the ratio between Fe-oxides and Fe-bound P is also apparently depth dependent; decreasing from approximately 3 at the sediment surface, to 1.8 below the SMTZ. This decrease indicates a depth-dependent change in the relative contribution of authigenic phases responsible for P sequestration. Consistent with observational and geochemical evidence for the presence of authigenic vivianite (Fig. 7a), the decrease in the Fe-oxide/Fe-bound P ratio to 1.8 approximates the stoichiometric Fe/P of vivianite (1.5), again advocating that vivianite authigenesis below the SMTZ is a potentially important process responsible for P burial at Site 973-4.

Previous studies have shown that vivianite dissolves in both the citrate-dithionite-bicarbonate (CDB; Nembrini et al., 1983) and dithionite steps (Dijkstra et al., 2014) of the sequential P- and Fe-extractions, respectively. Thus, both fractions contain P and Fe derived from vivianite (P_{viv} and Fe_{viv}) and Fe-oxides (P_{FeOx} and Fe_{FeOx}). Consequently, the total amount of P extracted during the CDB step is the sum of P_{viv} and P_{FeOx}, while the total amount of Fe extracted during the dithionite steps is the sum

of Fe_{viv} and Fe_{FeOx}. Combining these measured fractions with the Fe_{FeOx}/P_{FeOx} ratio of surface sediments at our site (~3) as a measure of P binding capacity and the stoichiometric Fe/P ratio of vivianite (1.5), we can estimate the quantitative importance of vivianite burial via the approach outlined by Egger et al. (2015a). Here, adopting average concentrations of Fe-bound P (108.3 µmol g^{-1}, Fig. 9b) and Fe-oxides (196.4 µmol g^{-1}, Fig. 8a) from below the sulfidization front at Site 973-4, a set of four equations, with an equal number of unknowns can be written:

$$Fe_{FeOx} + Fe_{viv} = 196.4 \text{ µmol } g^{-1} \quad \text{(Eq.2)}$$

$$P_{FeOx} + P_{viv} = 108.3 \text{ µmol } g^{-1} \quad \text{(Eq.3)}$$

$$Fe_{FeOx} = 3P_{FeOx} \quad \text{(Eq.4)}$$

$$Fe_{viv} = 1.5P_{viv} \quad \text{(Eq.5)}$$

Simultaneously solving these equations for Fe_{viv} and P_{viv} reveals that ~129 µmol g^{-1} of the Fe extracted during the dithionite extraction, along with ~86 µmol g^{-1} of the Fe-bound P, originated from vivianite, accounting for ~79% of the total Fe-bound P below the SMTZ. Authigenic Ca-P is the major P sink (~55%) at Site 973-4, in agreement with its globally estimated importance (~50%; Ruttenberg, 2014; Ruttenberg and Berner, 1993). Vivianite, by contrast, houses approximately 10% of the sub-SMTZ P inventory. These results further suggest that only 1 to 7.3% (average and maximum, n=70) of the chemically-constrained vivianite was recovered as coarse aggregates (Fig. 7a). This discrepancy, in turn, implies that much of the authigenic vivianite fraction is either disseminated as smaller crystals (< 65 µm) or as an amorphous solid-phase, as suggested previously by März et al. (2008a, 2018).

Vivianite plays an important role in Fe cycling below the SMTZ. The sediment column at Site 973-4 can be divided at ~900 cm depth, forming two distinct geochemical zones with different Fe, P and S systematics. Thus, several additional ratios can be calculated based on the previously discussed Fe- and P-extractions (Table 1). Total reactive Fe includes Fe-oxides and their authigenic reduction products (e.g., vivianite, pyrite and Fe carbonates). Considering that total Fe abundances (725 ± 30 µmol g^{-1}) are broadly invariant below 600 cm depth (Zhang et al., 2018b), and that the maximum AVS content (9.3 mmol g^{-1}) is one order of magnitude more abundant than total Fe, either we need to reconsider the quality of the AVS measurements (Zhang et al., 2014), or much of the quantified AVS (mainly H_2S + FeS) reflects dissolved sulfide, rather than Fe sulfides (Fig. 9b). Given the difficulties in deconvolving the relative importance of FeS and dissolved sulfide, coupled with the likely restriction of FeS to the sulfidization front at ~900 cm depth (Fig. 9b), FeS is precluded from further discussion.

Moving forward, this approach reveals that 52% of Fe-oxides were likely reduced to pyrite within the SMTZ, whereas 41% were converted to vivianite below the SMTZ. While vivianite may represent a major component of total P inventory below the SMTZ in coastal settings (40–50%; Egger et al., 2015a), its importance as an Fe sink is muted, representing only a small fraction of the of total reactive Fe budget in the Baltic Sea sediments (~6.4%; Rooze et al., 2016). At Site 973-4, however, vivianite accounts for almost half of the reactive Fe burial below the SMTZ, arguing that vivianite may represent an important Fe burial phase in methane-rich deep-sea sediments. Considering the concentrations of total Fe are broadly constant below 600 cm depth at Site 973-4, Fe reduction contributes similar amounts of Fe(II) (~34% and ~32% of total Fe) below and within the SMTZ providing the Fe(II) phases are authigenic. Hence, besides abiotic reductive dissolution of Fe-oxides within the SMTZ,

Fe cycling is strongly affected by Fe reduction at depth. Based on the discussion above, we argue that Fe-AOM is a likely source of reduced Fe, which may sequester around 34% of total Fe as a reduced burial phase below the SMTZ. Accordingly, bacterial Fe reduction coupled to AOM likely plays an important role for Fe and P cycling at depth.

While the detailed mineralogical work necessary to confirm the spatial importance of vivianite authigenesis in open marine sediments awaits, at least at Site 973-4, vivianite authigenesis proceeds below the SMTZ, driven apparently by deep Fe reduction which, in the absence of free sulfide, apparently supplies copious quantities of pore water Fe^{2+} and PO_4. Therefore, it follows that substantial burial of vivianite below the SMTZ associated with Fe reduction will have significantly altered the sedimentary record. Consequently, extra caution is warranted when using sedimentary P distributions of methane-rich sediments to reconstruct past ocean primary productivity and P burial pathways (Dijkstra et al., 2018a).

5.4 Long-term vivianite preservation—An outstanding question

The paleoenvironmental importance of vivianite in a geological sense depends on its longevity within the sediment pile. As discussed, vivianite is unstable in the presence of H_2S yet the presence of an SMTZ serves as an efficient sulfide trap, and thus may promote vivianite preservation at depth. Consequently, there may be deeper layers of vivianite preserved within the 3–4 km thick sediment package preserved in the Taixinan Basin (McDonnell et al., 2000). Naturally, however, this assumption requires that vivianite does not undergo any further down-core transformation.

At Site 973-4 authigenic Ca-P concentrations increase down core (Fig. 9c), which may reflect the conversion of more labile P-species into authigenic apatite. This sink switching is considered to be the globally significant driver of apatite authigenesis in marine sediments (e.g. Ruttenberg and Berner, 1993; Slomp et al., 1996). Whether vivianite is converted to authigenic apatite at depth, while possible, remains an open question. If it were a simple conversion, however, one would predict a linear increase in authigenic apatite at the expense of vivianite. Closer inspection of the relevant solid phase records reveals that this is not the case and, in fact, the relationship between apatite and vivianite concentrations is ambiguous at Site 973-4 (Figs. 7a and 9c). Alternatively, the apparent increase in authigenic Ca-P from the SMTZ to the bottom of the core may reflect non-vivianite-related apatite authigenesis at depth. Upward fluxes of Ca^{2+} and F^- to the SMTZ have been observed in continental margin settings (e.g. Clemens et al., 2016; März et al., 2018), which would provide the necessary chemical constituents to promote sub-SMTZ apatite authigenesis. If apatite was the more favorable PO_4 sink, then precipitation of this mineral phase could hypothetically curtail vivianite authigenesis. In this scenario, although the two phosphate phases are linked, they are linked through Ca^{2+}- and F^--availability rather than stability and conversion of one phase to another.

Besides potential transformation to authigenic apatite, vivianite is sensitive to oxidation and thus it is possible that vivianite in deep-time records has been transformed into Fe(III) phosphates (e.g. koninckite; März et al., 2008a), Fe-oxides (e.g. hematite; Berner, 1981), or some other unknown phase. Pseudomorphs of vivianite are apparently common in the deep-time record, providing at least some evidence for the transformation and stabilization of vivianite as it ages (e.g. metavivianite; Rodgers, 1986). Equally, however, the perceived absence of vivianite in aged sedimentary archives could be an artifact of insufficient surveys. Akin to März et al. (2018), we have shown that vivianite is a finely disseminated phase and thus may have escaped

detection in many studies. Moreover, typically employed extraction schemes co-extract vivianite, meaning that Fe-bound P in deep-time records could indeed have been wrongly ascribed, and could be vivianite (c.f., März et al., 2008b). Future work, targeting long cores, coupling aqueous- and solid-phase analysis, is required to definitively test our hypotheses linking vivianite authigenesis and Fe-AOM activity, as well as to examine the long-term stability of vivianite in the sedimentary record. More routine application of XRD analyses and modification of solid-phase extraction protocols is also necessary to more completely understand the geological significance of vivianite.

5.5 Phosphorous cycling through Earth history

The redox state of a given water mass is expected to profoundly influence P-cycling. For example, where basal waters are oxygenated, a similar pore water pattern to that observed at Site 973-4, or other modern open marine setting, is generally expected (Fig. 10), fostering vivianite authigenesis below the SMTZ. If oxygen concentrations drop, however, vivianite authigenesis is expected to be different with implications for P-cycling and productivity. Under ferruginous (anoxic and Fe^{2+}-rich) conditions, PO_4 would be adsorbed to and/or co-precipitated with Fe-oxides (März et al., 2008b), or even precipitated as vivianite directly if Fe^{2+} and PO_4 concentrations were sufficiently high (Dijkstra et al., 2018b). This P shuttle is, at least, partially eradicated if euxinic conditions develop in the water column, caused by sulfidization of Fe-oxides and/or vivianite. After settling, the fate of the P-rich Fe-oxides and vivianite particles would be dictated by the prevailing conditions in the diagenetic environment. Under sulfate limited conditions P removed from the water column is likely to be retained in the sediment, throttling productivity via a negative feedback (März et al., 2008b). When sulfate is available, however, reductive dissolution of Fe-oxides will liberate PO_4 to the pore water which may be lost or retained dependent on the locus of dissolution and the availability of other important dissolved species (Ca^{2+}, Fe^{2+}, Mg^{2+}, F^-) and reductants (e.g., organic matter, CH_4).

Applying these principles to our understanding of Earth History is somewhat speculative but nonetheless interesting, with broad implications for P-cycling. In the largely low-sulfate ferruginous oceans prior to the Great Oxidation Event (GOE; Lyons et al., 2014; Luo et al., 2016), the development of euxinia would have been scarce, enhancing PO_4 shuttling to the sediment. If this PO_4 was efficiently retained on a global-scale, then PO_4 availability in these ancient oceans would have been low, especially considering the reduction in oxidative weathering (Reinhard et al., 2017). By contrast, throughout Earth's history euxinic marine environments have become more prevalent—a consequence of rising sulfate concentrations (Poulton, 2017). As discussed, euxinic conditions are thought to promote P recycling and its return to the water column; whereas P is believed to be more recalcitrant in ferruginous environments. In a simple sense, therefore, euxinic conditions are touted to be quasi self-sustaining (via a productivity feedback) whereas ferruginous conditions are not. In a wider Earth System sense, however, these gross generalizations may not be valid, and warrant further investigation. Sustained euxinia, for example, could lower sulfate inventories favoring the development of ferruginous conditions if the S/Fe_{HR} ratio drops below 1.8 (e.g., Poulton and Canfield., 2011). Furthermore, unless reactive Fe enrichments are solely derived from hydrothermal emanations, simple mass balance constraints dictate that sedimentary Fe enrichments are unlikely to occur throughout an anoxic ocean and the source region must be depleted in reactive Fe (e.g., Poulton and Canfield., 2011). Accordingly, to understand the global effects of oxygen

deficiency on P-cycling we must more completely understand the local controls on P-cycling, and how oxygen deficiency developed on an event-by-event basis, to successfully integrate these processes in an Earth system model.

Interestingly, within the present-day oceans, sulfate-driven AOM is known to almost entirely consume methane, serving as an efficient sedimentary methane filter, and preventing this potent greenhouse gas from reaching the atmosphere (Egger et al., 2018; Knittel and Boetius, 2009). In the low sulfate pre-GOE oceans, however, sulfate scarcity may have limited methane oxidation, potentially allowing it to accumulate in the atmosphere (Habicht et al., 2002; Izon et al., 2015, 2017; Kasting et al., 2001). Against this sulfate-lean backdrop, the prevalence of Fe oxide-rich deposits known as banded iron formations (BIFs) dating from the Archean and early Paleoproterozoic (Klein, 2005; Konhauser et al., 2002), are testament to the ubiquity of Fe within the Earth's early oceans. It is possible, therefore, that Fe-AOM was a much more important process within Earth's oxygen deficient early oceans relative to their contemporary counterparts. If true, the interplay between Fe and methane, especially in the prelude of the GOE (e.g., Izon et al., 2017), could have modulated the methane efflux from the ocean to the atmosphere (Riedinger et al., 2014).

6 Conclusions

Combining bulk geochemical extractions with microscopic and spectroscopic analyses of handpicked mineral aggregates, we show that vivianite formation occurs within the iron- and methane-rich sediments from the Taixinan Basin, South China Sea. The identified vivianite aggregates are enriched in magnesium but are depleted in manganese, reflecting their growth environment. We argue that as the source of Fe^{2+} for vivianite authigenesis, Fe reduction below the SMTZ was probably driven by Fe-mediated anaerobic oxidation of methane, which has broad implications for Fe and P cycling at depth. Importantly, vivianite authigenesis appears to be restricted to sediments below the SMTZ, where it accounts for ~79% of the Fe-bound P and ~10% of the total sub-SMTZ P burial, respectively. Notably, we calculate that vivianite may account for almost half of the total reactive Fe burial below the SMTZ at Site 973-4. Geochemical conditions that characterize site 973-4 are not uncommon and typify continental margins (Kasten et al., 1998; März et al., 2008a; Riedinger et al., 2014). Thus, vivianite may be an important burial phase for P and Fe below the SMTZ in present-day marine systems (e.g. März et al., 2018). We further speculate that authigenic vivianite might have served as a significant P sink during episodes of marine oxygen deficiency (e.g., März et al., 2008b), throttling productivity via a negative feedback. Moreover, the interplay between Fe and methane, especially in the prelude of the GOE (e.g., Izon et al., 2017), could have curtailed marine methane fluxes with ramifications for the climate system (Riedinger et al., 2014). Thus, a better understanding of vivianite authigenesis is paramount to test long-standing hypotheses linking climate, atmospheric chemistry and the evolution of the biosphere.

Acknowledgements

Qi Lin is acknowledged for his insight into the study area; whereas formative discussions with Bo Barker Jørgensen, Samantha Joye and Alexandra V. Turchyn helped shape the preparation of this manuscript. We recognize technical assistance from Xiaoping Liao, Wanjun Lu, Chao Li, Caixiang Zhang, Xinna Chai, Jishun Yu, Zihu Zhang and Muhui Zhang at CUG, Wuhan. Daidai Wu, Jie Zhang and Wenjia Ou graciously shared data. The Guangzhou Marine Geological Survey, along with the crew and scientists on board R/V *Ocean VI* are acknowledged for sampling and logistical support. This research was funded by State Key R&D Project of China (Grant 2016YFA0601102), National Natural Science Foundation of China (Grants 41772091, 41472085 and 41802025) and China National Gas Hydrate Project (Grant DD20160211). JL acknowledges financial support via the international exchange program at the School of Earth Sciences, CUG. GI gratefully recognizes support from the Simons Foundation, who funded his contribution under the auspices of the Simons Collaboration on the Origin of Life. Travel support from CUG (Wuhan and Beijing) initiated this collaboration and ignited GI's interest in vivianite. Editorial handling by Tina Treude and reviews by Christian März and an anonymous reviewer are gratefully acknowledged: their expertise, insight and rigor have undoubtedly improved the clarity and quality of the final manuscript.

References

Algeo, T. J., and Ingall, E.: Sedimentary Corg:P ratios, paleocean ventilation, and Phanerozoic atmospheric pO2, Palaeogeogr., Palaeoclimatol., Palaeoecol., 256, 130-155, doi:10.1016/j.palaeo.2007.02.029, 2007.

Amonette, J. E., and Templeton, J. C.: Improvements to the quantitative assay of nonrefractory minerals for Fe (II) and total Fe using 1, 10-phenanthroline, Clays Clay Miner., 46, 51-62, doi:10.1346/CCMN.1998.0460106, 1998.

Amos, R., Bekins, B., Cozzarelli, I., Voytek, M., Kirshtein, J., Jones, E., and Blowes, D.: Evidence for iron-mediated anaerobic methane oxidation in a crude oil-contaminated aquifer, Geobiology, 10, 506-517, doi:10.1111/j.1472-4669.2012.00341.x, 2012.

Bar-Or, I., Elvert, M., Eckert, W., Kushmaro, A., Vigderovich, H., Zhu, Q., Ben-Dov, E., and Sivan, O.: Iron-Coupled Anaerobic Oxidation of Methane Performed by a Mixed Bacterial-Archaeal Community Based on Poorly Reactive Minerals, Environ. Sci. Technol., 51, 12293-12301, doi:10.1021/acs.est.7b03126, 2017.

Beal, E. J., House, C. H., and Orphan, V. J.: Manganese-and iron-dependent marine methane oxidation, Science, 325, 184-187, doi:10.1126/science.1169984, 2009.

Berner, R. A.: Thermodynamic stability of sedimentary iron sulfides, Am. J. Sci., 265, 773-785, doi:10.2475/ajs.265.9.773, 1967.

Berner, R. A.: A new geochemical classification of sedimentary environments, J. Sediment. Res., 51, 359-365, doi:10.1306/212F7C7F-2B24-11D7-8648000102C1865D, 1981.

Borowski, W. S., Paull, C. K., and Ussler III, W.: Marine pore-water sulfate profiles indicate in situ methane flux from underlying gas hydrate, Geology, 24, 655-658, doi:10.1130/0091-7613(1996)024<0655:MPWSPI>2.3.CO;2, 1996.

Borowski, W. S., Rodriguez, N. M., Paull, C. K., and Ussler III, W.: Are 34S-enriched authigenic sulfide minerals a proxy for elevated methane flux and gas hydrates in the geologic record?, Mar. Pet. Geol., 43, 381-395, doi:10.1016/j.marpetgeo.2012.12.009, 2013.

Burns, S.: Early diagenesis in Amazon fan sediments, in: Proc. ODP Sci. Results, edited by: Flood, R. D., Piper, D. J. W., Klaus, A., and Peterson, L. C., Texas, USA, 497-504, 1997.

Cai, C., Leu, A. O., Xie, G.-J., Guo, J., Feng, Y., Zhao, J.-X., Tyson, G. W., Yuan, Z., and Hu, S.: A methanotrophic archaeon couples anaerobic oxidation of methane to Fe(III) reduction, The ISME Journal, 12, 1929-1939, doi:10.1038/s41396-018-0109-x, 2018.

Canfield, D. E.: Reactive iron in marine sediments, Geochim. Cosmochim. Ac., 53, 619-632, doi:10.1016/0016-7037(89)90005-7, 1989.

Canfield, D. E., Raiswell, R., and Bottrell, S. H.: The reactivity of sedimentary iron minerals toward sulfide, Am. J. Sci., 292, 659-683, doi:10.2475/ajs.292.9.659, 1992.

Clemens, S. C., Kuhnt, W., LeVay, L. J., and the Expedition 353 Scientists: Indian Monsoon Rainfall. Proceedings of the International Ocean Discovery Program, 353, College Station, Texas, USA, doi:10.14379/iodp.proc.353.2016, 2016.

Crowe, S., Katsev, S., Leslie, K., Sturm, A., Magen, C., Nomosatryo, S., Pack, M., Kessler, J., Reeburgh, W., and Roberts, J.: The methane cycle in ferruginous Lake Matano, Geobiology, 9, 61-78, doi:10.1111/j.1472-4669.2010.00257.x, 2011.

Delaney, M.: Phosphorus accumulation in marine sediments and the oceanic phosphorus cycle, Global Biogeochem. Cycles, 12, 563-572, doi:10.1029/98GB02263, 1998.

Dijkstra, N., Kraal, P., Kuypers, M. M., Schnetger, B., and Slomp, C. P.: Are iron-phosphate minerals a sink for phosphorus in anoxic Black Sea sediments?, PloS one, 9, e101139, doi:10.1371/journal.pone.0101139, 2014.

Dijkstra, N., Slomp, C. P., and Behrends, T.: Vivianite is a key sink for phosphorus in sediments of the Landsort Deep, an intermittently anoxic deep basin in the Baltic Sea, Chem. Geol., 438, 58-72, doi:10.1016/j.chemgeo.2016.05.025, 2016.

Dijkstra, N., Hagens, M., Egger, M., and Slomp, C. P.: Post-depositional formation of vivianite-type minerals alters sediment phosphorus records, Biogeosciences, 15, 861-883, doi:10.5194/bg-2017-295, 2018a.

Dijkstra, N., Krupinski, N. B. Q., Yamane, M., Obrochta, S. P., Miyairi, Y., Yokoyama, Y., and Slomp, C. P.: Holocene refreshening and reoxygenation of a Bothnian Sea estuary led to enhanced phosphorus burial, Estuar. Coast., 41, 139-157, doi:10.1007/s12237-017-0262-x, 2018b.

Egger, M., Jilbert, T., Behrends, T., Rivard, C., and Slomp, C. P.: Vivianite is a major sink for phosphorus in methanogenic coastal surface sediments, Geochim. Cosmochim. Ac., 169, 217-235, doi:10.1016/j.gca.2015.09.012, 2015a.

Egger, M., Rasigraf, O., Sapart, C. l. J., Jilbert, T., Jetten, M. S., Röckmann, T., van der Veen, C., Bândă, N., Kartal, B., and Ettwig, K. F.: Iron-mediated anaerobic oxidation of methane in brackish coastal sediments, Environ. Sci. Technol., 49, 277-283, doi:10.1021/es503663z, 2015b.

Egger, M., Kraal, P., Jilbert, T., Sulu-Gambari, F., Sapart, C. J., Röckmann, T., and Slomp, C. P.: Anaerobic oxidation of methane alters sediment records of sulfur, iron and phosphorus in the Black Sea, Biogeosciences, 13, 5333-5355, doi:10.5194/bg-13-5333-2016, 2016.

Egger, M., Hagens, M., Sapart, C. J., Dijkstra, N., van Helmond, N. A., Mogollón, J. M., Risgaard-Petersen, N., van der Veen, C., Kasten, S., and Riedinger, N.: Iron oxide reduction in methane-rich deep Baltic Sea sediments, Geochim. Cosmochim. Ac., 207, 256-276, doi:10.1016/j.gca.2017.03.019, 2017.

Egger, M., Riedinger, N., Mogollón, J. M., and Jørgensen, B. B.: Global diffusive fluxes of methane in marine sediments, Nat. Geosci., doi:10.1038/s41561-018-0122-8, 2018.

Ettwig, K. F., Zhu, B., Speth, D., Keltjens, J. T., Jetten, M. S., and Kartal, B.: Archaea catalyze iron-dependent anaerobic oxidation of methane, P. Natl. Acad. Sci. USA, 113, 12792-12796, doi:10.1073/pnas.1609534113, 2016.

Fagel, N., Alleman, L., Granina, L., Hatert, F., Thamo-Bozso, E., Cloots, R., and André, L.: Vivianite formation and distribution in Lake Baikal sediments, Global Planet. Change, 46, 315-336, doi:10.1016/j.gloplacha.2004.09.022, 2005.

Feng, D., and Chen, D.: Authigenic carbonates from an active cold seep of the northern South China Sea: new insights into fluid sources and past seepage activity, Deep-Sea Res. Pt. II, 122, 74-83, doi:10.1016/j.dsr2.2015.02.003, 2015.

Feng, D., Cheng, M., Kiel, S., Qiu, J.-W., Yang, Q., Zhou, H., Peng, Y., and Chen, D.: Using Bathymodiolus tissue stable carbon, nitrogen and sulfur isotopes to infer biogeochemical process at a cold seep in the South China Sea, Deep-Sea Res. Pt. I, 104, 52-59, doi:10.1016/j.dsr.2015.06.011, 2015.

Feng, D., Qiu, J.-W., Hu, Y., Peckmann, J., Guan, H., Tong, H., Chen, C., Chen, J., Gong, S., Li, N., and Chen, D.: Cold seep systems in the South China Sea: An overview, J. Asian Earth Sci., doi:10.1016/j.jseaes.2018.09.021, 2018.

Grizelj, A., Bakrač, K., Horvat, M., Avanić, R., and Hećimović, I.: Occurrence of vivianite in alluvial Quaternary sediments in the area of Sesvete (Zagreb, Croatia), Geologia Croatica, 70, 41-52, doi:10.4154/gc.2017.01, 2017.

Habicht, K. S., Gade, M., Thamdrup, B., Berg, P., and Canfield, D. E.: Calibration of Sulfate Levels in the Archean Ocean, Science, 298, 2372-2374, doi:10.1126/science.1078265, 2002.

Haese, R. R., Wallmann, K., Dahmke, A., Kretzmann, U., Müller, P. J., and Schulz, H. D.: Iron species determination to investigate early diagenetic reactivity in marine sediments, Geochim. Cosmochim. Ac., 61, 63-72, doi:10.1016/S0016-7037(96)00312-2, 1997.

Han, X., Suess, E., Huang, Y., Wu, N., Bohrmann, G., Su, X., Eisenhauer, A., Rehder, G., and Fang, Y.: Jiulong methane reef: microbial mediation of seep carbonates in the South China Sea, Mar. Geol., 249, 243-256, doi:10.1016/j.margeo.2007.11.012, 2008.

Holmkvist, L., Ferdelman, T. G., and Jørgensen, B. B.: A cryptic sulfur cycle driven by iron in the methane zone of marine sediment (Aarhus Bay, Denmark), Geochim. Cosmochim. Ac., 75, 3581-3599, doi:10.1016/j.gca.2011.03.033, 2011.

Holmkvist, L., Kamyshny Jr, A., Bruechert, V., Ferdelman, T. G., and Jørgensen, B. B.: Sulfidization of lacustrine glacial clay upon Holocene marine transgression (Arkona Basin, Baltic Sea), Geochim. Cosmochim. Ac., 142, 75-94, doi:10.1016/j.gca.2014.07.030, 2014.

Hsu, H.-H., Liu, C.-S., Morita, S., Tu, S.-L., Lin, S., Machiyama, H., Azuma, W., Ku, C.-Y., and Chen, S.-C.: Seismic imaging of the Formosa Ridge cold seep site offshore of southwestern Taiwan, Mar. Geophys. Res., 1-13, doi:10.1007/s11001-017-9339-y, 2017.

Hsu, T.-W., Jiang, W.-T., and Wang, Y.: Authigenesis of vivianite as influenced by methane-induced sulfidization in cold-seep sediments off southwestern Taiwan, J. Asian Earth Sci., 89, 88-97, doi:10.1016/j.jseaes.2014.03.027, 2014.

Hu, Y., Feng, D., Liang, Q., Xia, Z., Chen, L., and Chen, D.: Impact of anaerobic oxidation of methane on the geochemical cycle of redox-sensitive elements at cold-seep sites of the northern South China Sea, Deep-Sea Res. Pt. II, 122, 84-94, doi:10.1016/j.dsr2.2015.06.012, 2015.

Izon, G., Zerkle, A. L., Zhelezinskaia, I., Farquhar, J., Newton, R. J., Poulton, S. W., Eigenbrode, J. L., and Claire, M. W.: Multiple oscillations in Neoarchaean atmospheric chemistry, Earth. Planet. Sci. Lett., 431, 264-273, doi:10.1016/j.epsl.2015.09.018, 2015.

Izon, G., Zerkle, A. L., Williford, K. H., Farquhar, J., Poulton, S. W., and Claire, M. W.: Biological regulation of atmospheric chemistry en route to planetary oxygenation, P. Natl. Acad. Sci. USA, 114, E2571-E2579, doi:10.1073/pnas.1618798114, 2017.

Jensen, H. S., Mortensen, P. B., Andersen, F., Rasmusse, E., and Jensen, A.: Phosphorus cycling in a coastal marine sediment, Aarhus Bay, Denmark, Limnol. Oceanogr., 40, 908-917, doi:10.4319/lo.1995.40.5.0908, 1995.

Jørgensen, B. B., Böttcher, M. E., Lüschen, H., Neretin, L. N., and Volkov, I. I.: Anaerobic methane oxidation and a deep H2S sink generate isotopically heavy sulfides in Black Sea sediments, Geochim. Cosmochim. Ac., 68, 2095-2118, doi:10.1016/j.gca.2003.07.017, 2004.

Kagan, M. R., and McCreery, R. L.: Reduction of fluorescence interference in Raman spectroscopy via analyte adsorption on graphitic carbon, Anal. Chem., 66, 4159-4165, doi:10.1021/ac00095a008, 1994.

Kasten, S., Freudenthal, T., Gingele, F. X., and Schulz, H. D.: Simultaneous formation of iron-rich layers at different redox boundaries in sediments of the Amazon deep-sea fan, Geochim. Cosmochim. Ac., 62, 2253-2264, doi:10.1016/S0016-7037(98)00093-3, 1998.

Kasting, J. F., Pavlov, A. A., and Siefert, J. L.: A Coupled Ecosystem-Climate Model for Predicting the Methane Concentration in the Archean Atmosphere, Origins Life Evol. Biosphere, 31, 271-285, doi:10.1023/a:1010600401718, 2001.

Kennett, J. P., Cannariato, K. G., Hendy, I. L., and Behl, R. J.: Methane Hydrates in Quaternary Climate Change: The Clathrate Gun Hypothesis, American Geophysical Union, Washington, DC, USA, 2003.

Klein, C.: Some Precambrian banded iron-formations (BIFs) from around the world: Their age, geologic setting, mineralogy, metamorphism, geochemistry, and origins, Am. Mineral., 90, 1473-1499, doi:10.2138/am.2005.1871, 2005.

Knittel, K., and Boetius, A.: Anaerobic oxidation of methane: progress with an unknown process, Annu. Rev. Microbiol., 63, 311-334, doi:10.1146/annurev.micro.61.080706.093130, 2009.

Konhauser, K. O., Hamade, T., Raiswell, R., Morris, R. C., Ferris, F. G., Southam, G., and Canfield, D. E.: Could bacteria have formed the Precambrian banded iron formations?, Geology, 30, 1079-1082, doi:10.1130/0091-7613(2002)030<1079:CBHFTP>2.0.CO;2, 2002.

Kvenvolden, K. A.: Gas hydrates—geological perspective and global change, Rev. Geophys., 31, 173-187, doi:10.1029/93RG00268 1993.

Lin, Q., Wang, J., Fu, S., Lu, H., Bu, Q., Lin, R., and Sun, F.: Elemental sulfur in northern South China Sea sediments and its significance, Sci. China Earth Sci., 58, 2271-2278, doi:10.1007/s11430-015-5182-7, 2015.

Lin, Q., Wang, J., Algeo, T. J., Sun, F., and Lin, R.: Enhanced framboidal pyrite formation related to anaerobic oxidation of methane in the sulfate-methane transition zone of the northern South China Sea, Mar. Geol., 379, 100-108, doi:10.1016/j.margeo.2016.05.016, 2016a.

Lin, R., Wang, J., Su, P., Lin, Q., Sun, F., and Yang, J.: Characteristics of magnetic susceptibility of cored sediments and their implications for the potential methane events in northern South China Sea, Acta Sedimentologica Sinica, 35, 290-298, doi:10.14027/j.cnki.cjxb.2017.02.008, 2017a.

Lin, Z., Sun, X., Peckmann, J., Lu, Y., Xu, L., Strauss, H., Zhou, H., Gong, J., Lu, H., and Teichert, B. M. A.: How sulfate-driven anaerobic oxidation of methane affects the sulfur isotopic composition of pyrite: A SIMS study from the South China Sea, Chem. Geol., 440, 26-41, doi:10.1016/j.chemgeo.2016.07.007, 2016b.

Lin, Z., Sun, X., Strauss, H., Lu, Y., Gong, J., Xu, L., Lu, H., Teichert, B. M., and Peckmann, J.: Multiple sulfur isotope constraints on sulfate-driven anaerobic oxidation of methane: Evidence from authigenic pyrite in seepage areas of the South China Sea, Geochim. Cosmochim. Ac., 211, 153-173, doi:10.1016/j.gca.2017.05.015, 2017b.

Liu, C.-S., Huang, I. L., and Teng, L. S.: Structural features off southwestern Taiwan, Mar. Geol., 137, 305-319, doi:10.1016/S0025-3227(96)00093-X, 1997.

Lovley, D. R.: Microbial Fe (III) reduction in subsurface environments, FEMS Microbiol. Rev., 20, 305-313, doi:10.1111/j.1574-6976.1997.tb00316.x, 1997.

Lu, H., Liu, J., Chen, F., Cheng, S., and Liao, Z.: Shallow sulfate-methane interface in northeastern South China Sea: An indicator of strong methane seepage on seafloor, Mar Geol Quat Geol, 32, 93-98, doi:10.3724/SP.J.1140.2012.01093, 2012.

Luo, G., Ono, S., Beukes, N. J., Wang, D. T., Xie, S., and Summons, R. E.: Rapid oxygenation of Earth's atmosphere 2.33 billion years ago, Science Advances, 2, doi:10.1126/sciadv.1600134, 2016.

Lyons, T. W., Reinhard, C. T., and Planavsky, N. J.: The rise of oxygen in Earth's early ocean and atmosphere, Nature, 506, 307, doi:10.1038/nature13068, 2014.

März, C., Hoffmann, J., Bleil, U., De Lange, G., and Kasten, S.: Diagenetic changes of magnetic and geochemical signals by anaerobic methane oxidation in sediments of the Zambezi deep-sea fan (SW Indian Ocean), Mar. Geol., 255, 118-130, doi:10.1016/j.margeo.2008.05.013, 2008a.

März, C., Poulton, S. W., Beckmann, B., Küster, K., Wagner, T., and Kasten, S.: Redox sensitivity of P cycling during marine black shale formation: Dynamics of sulfidic and anoxic, non-sulfidic bottom waters, Geochim. Cosmochim. Ac., 72, 3703-3717, doi:10.1016/j.gca.2008.04.025, 2008b.

März, C., Riedinger, N., Sena, C., and Kasten, S.: Phosphorus dynamics around the sulphate-methane transition in continental margin sediments: Authigenic apatite and Fe(II) phosphates, Mar. Geol., 404, 84-96, doi:10.1016/j.margeo.2018.07.010, 2018.

Maslin, M., Owen, M., Day, S., and Long, D.: Linking continental-slope failures and climate change: Testing the clathrate gun hypothesis, Geology, 32, 53-56, doi:10.1130/G20114.1, 2004.

McDonnell, S., Max, M., Cherkis, N. e. a., and Czarnecki, M.: Tectono-sedimentary controls on the likelihood of gas hydrate occurrence near Taiwan, Mar. Pet. Geol., 17, 929-936, doi:10.1016/S0264-8172(00)00023-4, 2000.

McGlynn, S. E., Chadwick, G. L., Kempes, C. P., and Orphan, V. J.: Single cell activity reveals direct electron transfer in methanotrophic consortia, Nature, 526, 531, doi:10.1038/nature15512, 2015.

Morse, J. W.: Interactions of trace metals with authigenic sulfide minerals: implications for their bioavailability, Mar. Chem., 46, 1-6, doi:10.1016/0304-4203(94)90040-X, 1994.

Nakano, S.: Manganoan vivianite in the bottom sediments of Lake Biwa, Japan, Mineralogical Journal, 16, 96-107, doi:10.2465/minerj.16.96, 1992.

Nembrini, G., Capobianco, J., Viel, M., and Williams, A.: A Mössbauer and chemical study of the formation of vivianite in sediments of Lago Maggiore (Italy), Geochim. Cosmochim. Ac., 47, 1459-1464, doi:10.1016/0016-7037(83)90304-6, 1983.

Norði, K. à., Thamdrup, B., and Schubert, C. J.: Anaerobic oxidation of methane in an iron-rich Danish freshwater lake sediment, Limnol. Oceanogr., 58, 546-554, doi:10.4319/lo.2013.58.2.0546, 2013.

Nriagu, J. O.: Stability of vivianite and ion-pair formation in the system Fe3(PO4)2-H3PO4-H2O, Geochim. Cosmochim. Ac., 36, 459-470, doi:10.1016/0016-7037(72)90035-X, 1972.

Ou, W.: Sedimentary organic geochemistry research of source rocks of the potential gas hydrate-bearing areas in the northern South China Sea, Ph.D. thesis, Xiamen University, China, 2013.

Peckmann, J., and Thiel, V.: Carbon cycling at ancient methane–seeps, Chem. Geol., 205, 443-467, doi:10.1016/j.chemgeo.2003.12.025, 2004.

Piriou, B., and Poullen, J.: Raman study of vivianite, J. Raman Spectrosc., 15, 343-346, doi:10.1002/jrs.1250150510, 1984.

Porrenga, D. H.: Glauconite and chamosite as depth indicators in the marine environment, Mar. Geol., 5, 495-501, doi:10.1016/0025-3227(67)90056-4, 1967.

Poulton, S. W., Krom, M. D., and Raiswell, R.: A revised scheme for the reactivity of iron (oxyhydr) oxide minerals towards dissolved sulfide, Geochim. Cosmochim. Ac., 68, 3703-3715, doi:10.1016/j.gca.2004.03.012, 2004.

Poulton, S. W., and Canfield, D. E.: Development of a sequential extraction procedure for iron: implications for iron partitioning in continentally derived particulates, Chem. Geol., 214, 209-221, doi:10.1016/j.chemgeo.2004.09.003, 2005.

Poulton, S. W., and Canfield, D. E.: Ferruginous Conditions: A Dominant Feature of the Ocean through Earth's History, Elements, 7, 107-112, doi:10.2113/gselements.7.2.107, 2011.

Poulton, S. W.: Early phosphorus redigested, Nat. Geosci., 10, 75, doi:10.1038/ngeo2884, 2017.

Raiswell, R., Canfield, D., and Berner, R.: A comparison of iron extraction methods for the determination of degree of pyritisation and the recognition of iron-limited pyrite formation, Chem. Geol., 111, 101-110, doi:10.1016/0009-2541(94)90084-1, 1994.

Reed, D. C., Gustafsson, B. G., and Slomp, C. P.: Shelf-to-basin iron shuttling enhances vivianite formation in deep Baltic Sea sediments, Earth. Planet. Sci. Lett., 434, 241-251, doi:10.1016/j.epsl.2015.11.033, 2016.

Reinhard, C. T., Planavsky, N. J., Gill, B. C., Ozaki, K., Robbins, L. J., Lyons, T. W., Fischer, W. W., Wang, C., Cole, D. B., and Konhauser, K. O.: Evolution of the global phosphorus cycle, Nature, 541, 386, doi:10.1038/nature20772, 2017.

Riedinger, N., Formolo, M. J., Lyons, T. W., Henkel, S., Beck, A., and Kasten, S.: An inorganic geochemical argument for coupled anaerobic oxidation of methane and iron reduction in marine sediments, Geobiology, 12, 172-181, doi:10.1111/gbi.12077, 2014.

Riedinger, N., Brunner, B., Krastel, S., Arnold, G. L., Wehrmann, L. M., Formolo, M. J., Beck, A., Bates, S. M., Henkel, S., and Kasten, S.: Sulfur cycling in an iron oxide-dominated, dynamic marine depositional system: The Argentine continental margin, Front. Earth Sci., 5, 33, doi:10.3389/feart.2017.00033, 2017.

Rodgers, K. A.: Metavivianite and kerchenite: a review, Mineral. Mag., 50, 687-691, doi:10.1180/minmag.1986.050.358.16, 1986.

Rooze, J., Egger, M., Tsandev, I., and Slomp, C. P.: Iron-dependent anaerobic oxidation of methane in coastal surface sediments: Potential controls and impact, Limnol. Oceanogr., 61, doi:10.1002/lno.10275, 2016.

Rotaru, A.-E., and Thamdrup, B.: A new diet for methane oxidizers, Science, 351, 658-658, doi:10.1126/science.aaf0741, 2016.

Rothe, M., Eder, M., Kleeberg, A., and Hupfer, M.: Evidence for vivianite formation and its contribution to long-term phosphorus retention in a recent lake sediment: a novel analytical approach, Biogeosciences, 5169, doi:10.5194/bg-11-5169-2014, 2014.

Rothe, M., Kleeberg, A., Grüneberg, B., Friese, K., Pérez-Mayo, M., and Hupfer, M.: Sedimentary sulphur: iron ratio indicates vivianite occurrence: a study from two contrasting freshwater systems, Plos one, 10, e0143737, doi:10.1371/journal.pone.0143737, 2015.

Rothe, M., Kleeberg, A., and Hupfer, M.: The occurrence, identification and environmental relevance of vivianite in waterlogged soils and aquatic sediments, Earth-Sci. Rev., 158, 51-64, doi:10.1016/j.earscirev.2016.04.008, 2016.

Ruppel, C. D., and Kessler, J. D.: The interaction of climate change and methane hydrates, Rev. Geophys., 55, 126-168, doi:10.1002/2016RG000534, 2017.

Ruttenberg, K. C.: Development of a sequential extraction method for different forms of phosphorus in marine sediments, Limnol. Oceanogr., 37, 1460-1482, doi:10.4319/lo.1992.37.7.1460, 1992.

Ruttenberg, K. C., and Berner, R. A.: Authigenic apatite formation and burial in sediments from non-upwelling, continental margin environments, Geochim. Cosmochim. Ac., 57, 991-1007, doi:10.1016/0016-7037(93)90035-U, 1993.

Ruttenberg, K. C.: The Global Phosphorus Cycle, in: Treatise on Geochemistry (Second Edition), edited by: Turekian, K. K., Elsevier, Oxford, 499-558, 2014.

Sapota, T., Aldahan, A., and Al-Aasm, I. S.: Sedimentary facies and climate control on formation of vivianite and siderite microconcretions in sediments of Lake Baikal, Siberia, J. Paleolimnol., 36, 245-257, doi:10.1007/s10933-006-9005-x, 2006.

Scheller, S., Yu, H., Chadwick, G. L., McGlynn, S. E., and Orphan, V. J.: Artificial electron acceptors decouple archaeal methane oxidation from sulfate reduction, Science, 351, 703-707, doi:10.1126/science.aad7154, 2016.

Schulz, H. D., Dahmke, A., Schinzel, U., Wallmann, K., and Zabel, M.: Early diagenetic processes, fluxes, and reaction rates in sediments of the South Atlantic, Geochim. Cosmochim. Ac., 58, 2041-2060, doi:10.1016/0016-7037(94)90284-4, 1994.

Segarra, K. E., Comerford, C., Slaughter, J., and Joye, S. B.: Impact of electron acceptor availability on the anaerobic oxidation of methane in coastal freshwater and brackish wetland sediments, Geochim. Cosmochim. Ac., 115, 15-30, doi:10.1016/j.gca.2013.03.029, 2013.

Severmann, S., Johnson, C. M., Beard, B. L., and McManus, J.: The effect of early diagenesis on the Fe isotope compositions of porewaters and authigenic minerals in continental margin sediments, Geochim. Cosmochim. Ac., 70, doi:10.1016/j.gca.2006.01.007, 2006.

Sha, Z., Liang, J., Zhang, G., Yang, S., Lu, J., Zhang, Z., McConnell, D. R., and Humphrey, G.: A seepage gas hydrate system in northern South China Sea: Seismic and well log interpretations, Mar. Geol., 366, 69-78, doi:10.1016/j.margeo.2015.04.006, 2015.

Shi, C., Lei, H., Zhao, J., Zhang, J., and Han, C.: Vertical microbial community structure characteristics of sediment in gas hydrate potential area of northern South China Sea Jiulong Methane Reef, Acta Sedimentol Sinica, 32, 1072-1082, 2014.

Sivan, O., Adler, M., Pearson, A., Gelman, F., Bar-Or, I., John, S. G., and Eckert, W.: Geochemical evidence for iron-mediated anaerobic oxidation of methane, Limnol. Oceanogr., 56, 1536-1544, doi:10.4319/lo.2011.56.4.1536, 2011.

Slomp, C. P., Epping, E. H., Helder, W., and Raaphorst, W. V.: A key role for iron-bound phosphorus in authigenic apatite formation in North Atlantic continental platform sediments, J. Mar. Res., 54, 1179-1205, doi:10.1357/0022240963213745, 1996.

Slomp, C. P., Mort, H. P., Jilbert, T., Reed, D. C., Gustafsson, B. G., and Wolthers, M.: Coupled dynamics of iron and phosphorus in sediments of an oligotrophic coastal basin and the impact of anaerobic oxidation of methane, PloS one, 8, e62386, doi:10.1371/journal.pone.0062386, 2013.

Suess, E., Huang, Y., Wu, N., Han, X., and Su, X.: South China Sea continental margin: Geological methane budget and environmental effects of methane emissions and gas hydrates, RV SONNE Cruise Report, Leibniz Institute of Marine Sciences, Kiel, Germany, 1-154, 2005.

Sundby, B., Gobeil, C., Silverberg, N., and Alfonso, M.: The phosphorus cycle in coastal marine sediments, Limnol. Oceanogr., 37, 1129-1145, doi:10.4319/lo.1992.37.6.1129, 1992.

Tenzer, R., and Gladkikh, V.: Assessment of density variations of marine sediments with ocean and sediment depths, The Sci. World J., 2014, doi:10.1155/2014/823296, 2014.

Treude, T., Niggemann, J., Kallmeyer, J., Wintersteller, P., Schubert, C. J., Boetius, A., and Jørgensen, B. B.: Anaerobic oxidation of methane and sulfate reduction along the Chilean continental margin, Geochim. Cosmochim. Ac., 69, 2767-2779, doi:10.1016/j.gca.2005.01.002, 2005.

Treude, T., Krause, S., Maltby, J., Dale, A. W., Coffin, R., and Hamdan, L. J.: Sulfate reduction and methane oxidation activity below the sulfate-methane transition zone in Alaskan Beaufort Sea continental margin sediments: Implications for deep sulfur cycling, Geochim. Cosmochim. Ac., 144, 217-237, doi:10.1016/j.gca.2014.08.018, 2014.

Wallmann, K., Hennies, K., König, I., Petersen, W., and Knauth, H.-D.: New procedure for determining reactive Fe(III) and Fe(II) minerals in sediments, Limnol. Oceanogr., 38, 1803-1812, doi:10.4319/lo.1993.38.8.1803, 1993.

Wankel, S. D., Adams, M. M., Johnston, D. T., Hansel, C. M., Joye, S. B., and Girguis, P. R.: Anaerobic methane oxidation in metalliferous hydrothermal sediments: influence on carbon flux and decoupling from sulfate reduction, Environ. Microbiol., 14, 2726-2740, doi:10.1111/j.1462-2920.2012.02825.x, 2012.

Wegener, G., Krukenberg, V., Riedel, D., Tegetmeyer, H. E., and Boetius, A.: Intercellular wiring enables electron transfer between methanotrophic archaea and bacteria, Nature, 526, 587, doi:10.1038/nature15733, 2015.

Yan, Z., Joshi, P., Gorski, C. A., and Ferry, J. G.: A biochemical framework for anaerobic oxidation of methane driven by Fe (III)-dependent respiration, Nat. commun., 9, doi:10.1038/s41467-018-04097-9, 2018.

Ye, H., Yang, T., Zhu, G., Jiang, S., and Wu, L.: Pore water geochemistry in shallow sediments from the northeastern continental slope of the South China Sea, Mar. Pet. Geol., 75, 68-82, doi:10.1016/j.marpetgeo.2016.03.010, 2016.

Zhang, B., Wu, D., and Wu, N.: Characteristics of sedimentary geochemistry and their responses to cold-seep activities in Dongsha, the northern South China Sea, Marine Geology Frontiers, 31, 14-27, 2015a.

Zhang, B., Pan, M., Wu, D., and Wu, N.: Distribution and isotopic composition of foraminifera at cold-seep Site 973-4 in the Dongsha area, northeastern South China Sea, J. Asian Earth Sci., doi:10.1016/j.jseaes.2018.05.007, 2018a.

Zhang, G., Liang, J., Lu, J. a., Yang, S., Zhang, M., Holland, M., Schultheiss, P., Su, X., Sha, Z., and Xu, H.: Geological features, controlling factors and potential prospects of the gas hydrate occurrence in the east part of the Pearl River Mouth Basin, South China Sea, Mar. Pet. Geol., 67, 356-367, doi:10.1016/j.marpetgeo.2015.05.021, 2015b.

Zhang, J., Lei, H., Ou, W., Yang, Y., Gong, C., and Shi, C.: Research of the sulfate-methane transition zone (SMTZ) in sediments of 973-4 column in continental slope of northern South China Sea, Natural Gas Geoscience, 25, 1811-1820, doi:10.11764/j.issn.1672-1926.2014.11.1811, 2014.

Zhang, J., Lei, H., Yang, M., Chen, Y., Kong, Y., and Lu, Y.: The Interactions of P-S-Fe in sediment from the continental slope of northern South China Sea and their implication for the sulfate – methane transition zone, Earth Sci. Front., 25, 285-293, doi:10.13745/j.esf.sf.2018.2.2, 2018b.

Zhang, J., Lei, H., Chen, Y., Kong, Y., Kandasamy, S., Ou, W., and Cheng, W.: Carbon and oxygen isotope composition of carbonate in bulk sediment in the southwest Taiwan Basin, south China sea: Methane hydrate decomposition history and its link to mud volcano eruption, Mar. Pet. Geol., doi:10.1016/j.marpetgeo.2018.08.031, 2018c.

Zhang, Z., Li, C., Cheng, M., Algeo, T. J., Jin, C., Tang, F., and Huang, J.: Evidence for Highly Complex Redox Conditions and Strong Water-Column Stratification in an Early Cambrian Continental-Margin Sea, Geochem. Geophys. Geosyst., 19, 2397-2410, doi:10.1029/2018GC007666, 2018d.

Zhong, G., Cartigny, M. J., Kuang, Z., and Wang, L.: Cyclic steps along the South Taiwan Shoal and West Penghu submarine canyons on the northeastern continental slope of the South China Sea, GSA Bulletin, 127, 804-824, doi:10.1130/B31003.1, 2015.

Zhuang, C., Chen, F., Cheng, S., Lu, H., Zhou, Y., and Liu, G.: Stable isotopic characteristics and their influencing factors of benthic foraminifera in the prospective gas hydrate area from the northern South China Sea since the last glacial, Quaternary Sciences, 35, 422-432, doi:10.11928/j.issn.1001-7410.2015.02.17, 2015.

Table

Table 1: Concentrations of specific Fe phases and their ratio to both total reactive Fe and total Fe at Site 973-4. Concentrations of Fe carbonates are taken from Zhang et al. (2018b).

Fe burial phase	Concentration below SMTZ ($\mu mol\ g^{-1}$)	Concentration in SMTZ ($\mu mol\ g^{-1}$)	Fe (II)/total reactive Fe below SMTZ	Fe (II)/total reactive Fe in SMTZ	Fe (II) /total Fe below SMTZ	Fe (II) /total Fe in SMTZ
Vivianite	129	N.A.	41%	N.A.	34%	32%
Pyrite	4	177	1%	52%		
Fe carbonates	111	54	36%	16%		
Total reactive Fe	311	341				

Figures

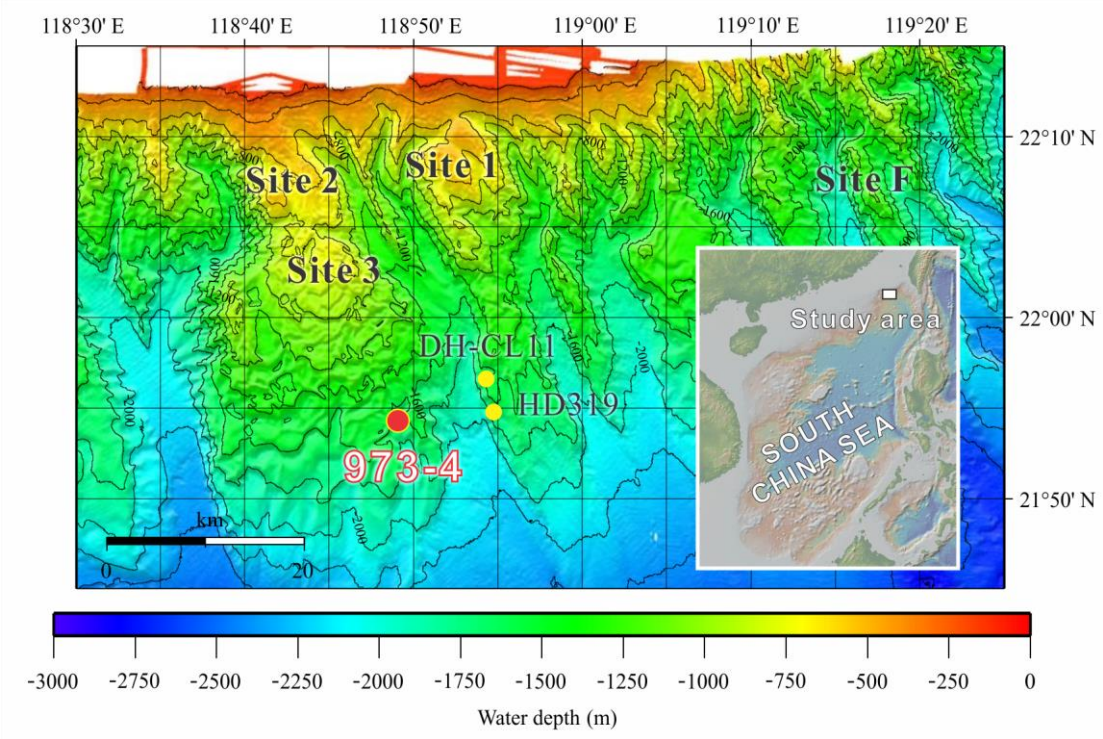

Figure 1: Bathymetric map locating Site 973-4 (red circle) with a geographical insert showing the Taixinan Basin within the wider South China Sea (after Suess et al., 2005).

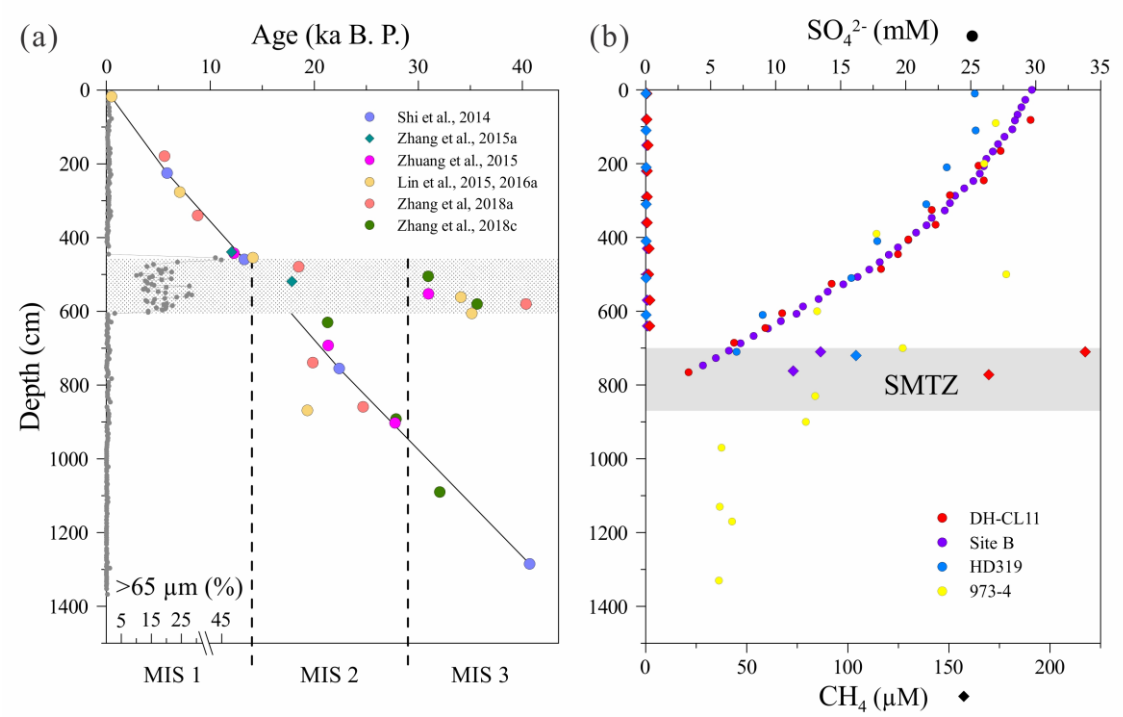

Figure 2: (a) Stratigraphic distribution of the coarse fraction (> 65 µm, Lin et al., 2017a) and radiocarbon- or $\delta^{18}O$-derived age datums from Site 973-4. (b) Profiles of interstitial sulfate (circles) and methane (diamonds) concentrations from Site 973-4 (Zhang et al., 2014) and other adjacent Sites (Lin et al., 2017b; Lu et al., 2012; Ye et al., 2016). Age constraints are either AMS ^{14}C dates derived from planktonic foraminifera (circles) in calendar years B.P. (Lin et al., 2015, 2016a; Shi et al., 2014; Zhang et al., 2018a; Zhang et al., 2018c; Zhuang et al., 2015) or via correlation to the LR04 benthic oxygen isotope stack (diamonds; Zhang et al., 2015a). MIS—Marine isotope stage. The headspace methane concentrations from Site B and HD 319 were calculated assuming the density of the wet sediments was 1.7 g cm^{-3} (Tenzer and Gladkikh, 2014). The horizontal bars in a and b represent either the coarse layer or the SMTZ, respectively.

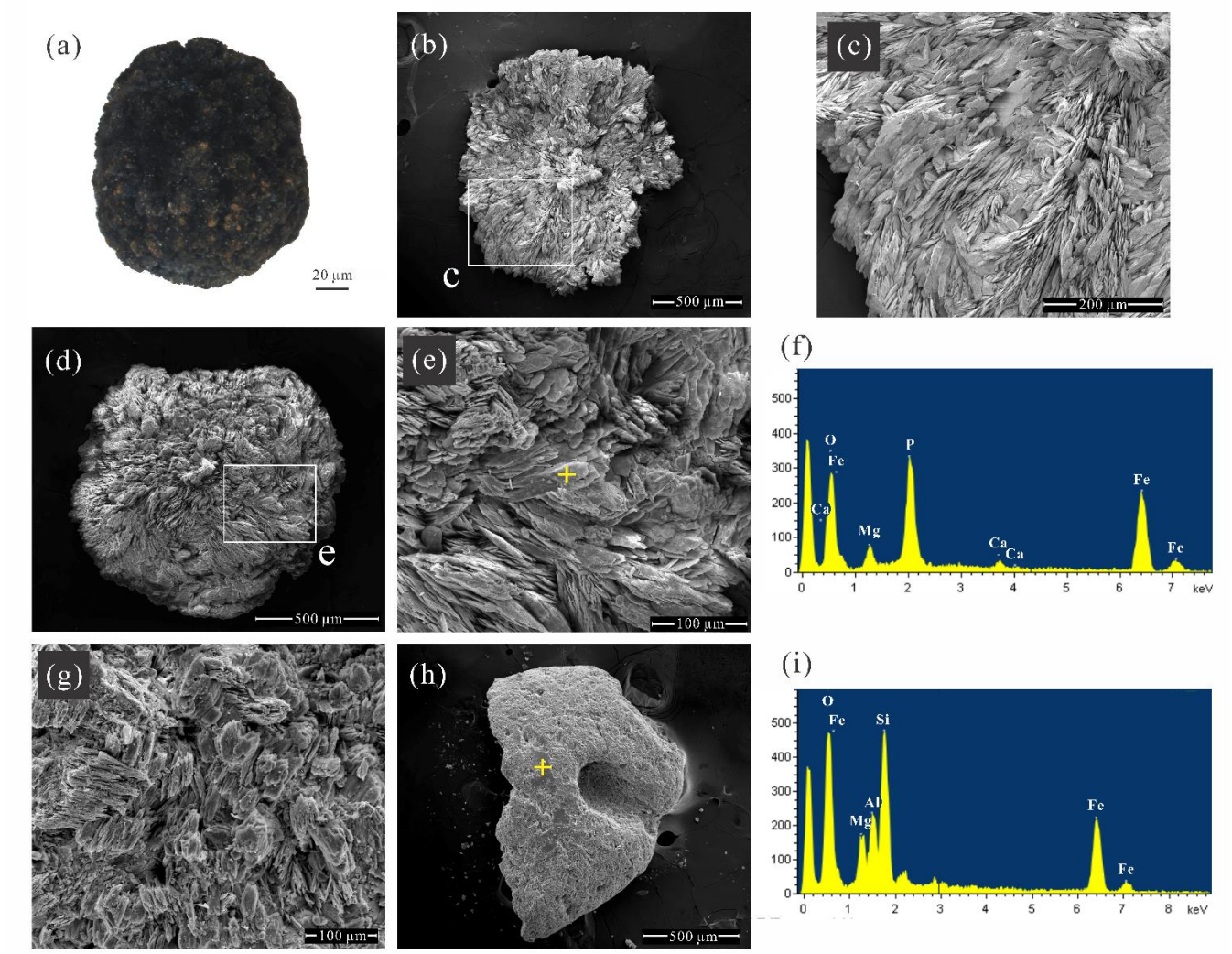

Figure 3: Images and chemical analyses of handpicked mineral aggregates from core 973-4. (a) Optical photomicrograph of an opaque dark mineral aggregate. (b−e, g) Scanning electron photomicrographs of the blue to black mineral aggregates found beneath the SMTZ. Samples b, d, g were handpicked from sediments at 1087.5, 1093.5, and 973.5 cm depth, respectively. The white boxes in b, d correspond to the fields of view enlarged c and e, respectively. (f) A spot-measurement EDS spectrum corresponding to the yellow cross in e. (h) Scanning electron photomicrograph of the grey to green mineral aggregates from sediments at 602.5 cm depth. (i) A spot-measurement EDS spectrum corresponding to the yellow cross in h.

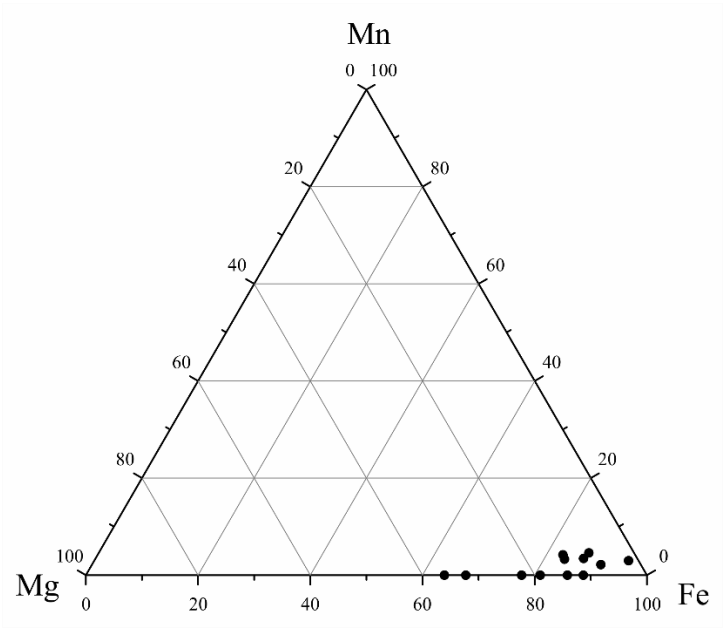

Figure 4: Ternary plot of the Fe–Mg–Mn contents (in wt.%) of the blue to black mineral aggregates isolated from sediments below the SMTZ. These data were derived from multiple EDS measurements.

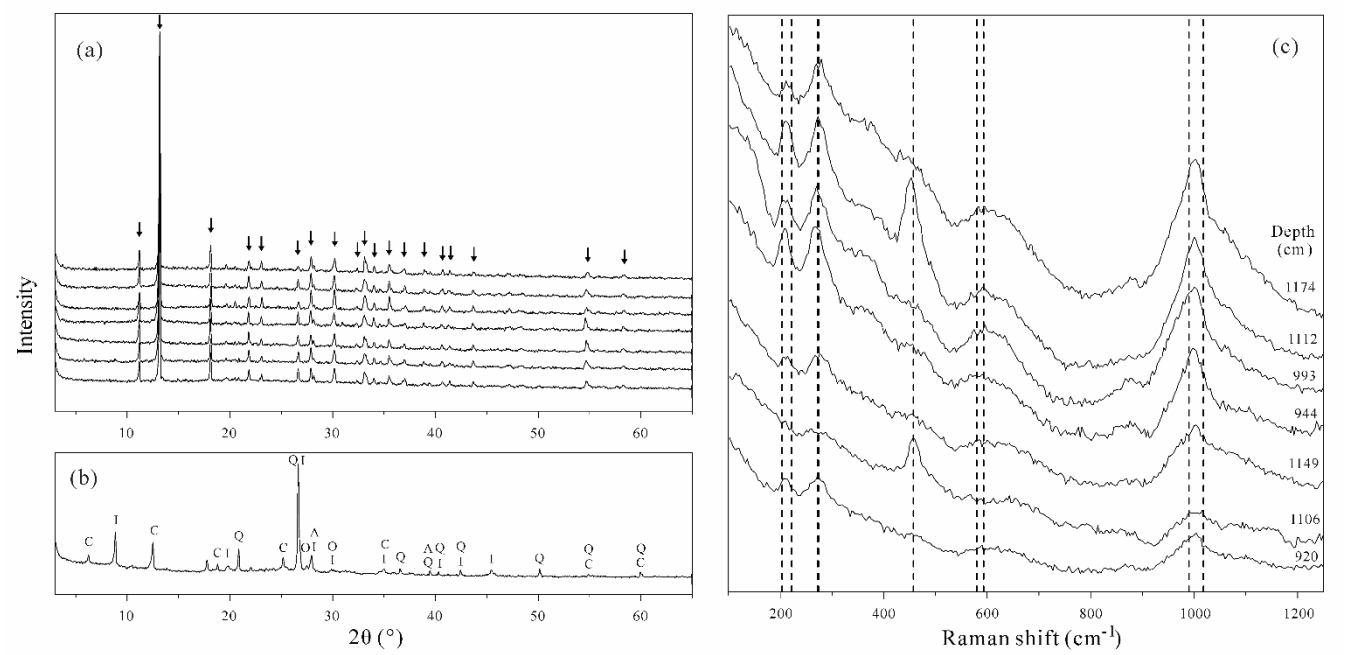

Figure 5: X-ray diffraction and Raman spectra of handpicked mineral aggregates. (a) XRD spectra of the blue to black mineral aggregates isolated from sediments from below the SMTZ. The spectra of samples from the top to the bottom correspond to samples taken at 920, 944, 993, 1106, 1112, 1149, and 1175 cm depth, respectively. All the identified peaks highlighted by arrows belong to the vivianite reference spectrum. (b) XRD spectrum of the grey to green mineral aggregates obtained from sediments at 1281 cm depth. I = illite, C = chlorites, Q = quartz, A = albite, O = orthoclase. (c) Raman spectra of the blue to black mineral aggregates from below the SMTZ. The dashed lines represent known vivianite spectral features (Piriou and Poullen, 1984).

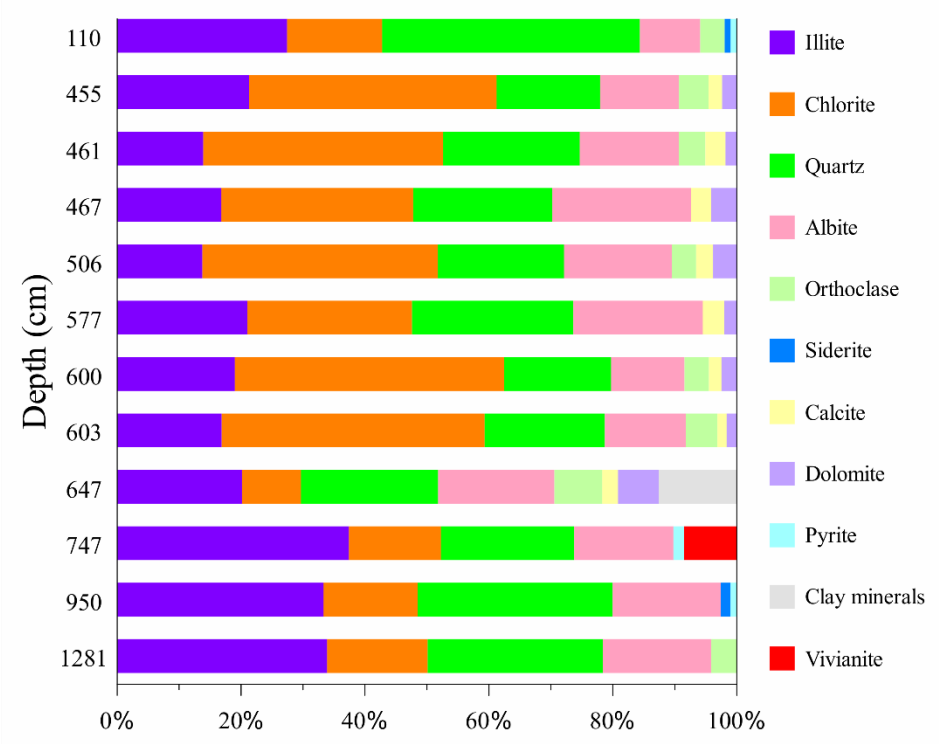

Figure 6: XRD derived depth profiles depicting the relative mineralogy of the grey to green mineral aggregates isolated from core 973-4. Some of the clay minerals from the sample at 647 cm depth remain unclassified.

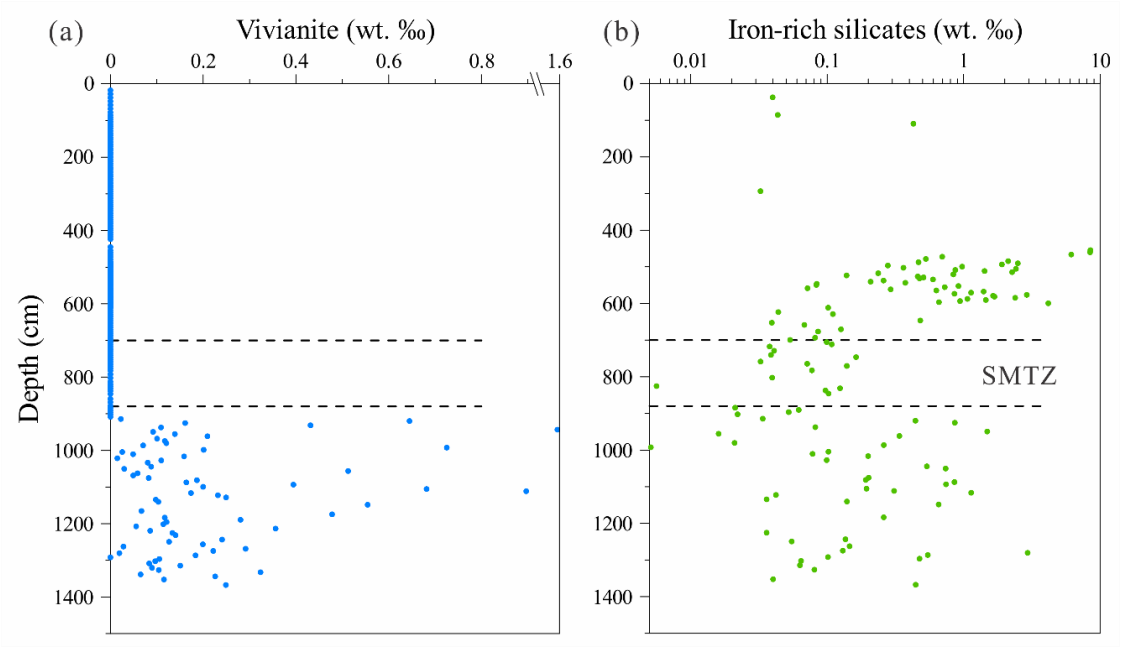

Figure 7: Depth distribution profiles of handpicked (a) vivianite, (b) Fe-rich silicates. The SMTZ is indicated by horizontal dashed lines.

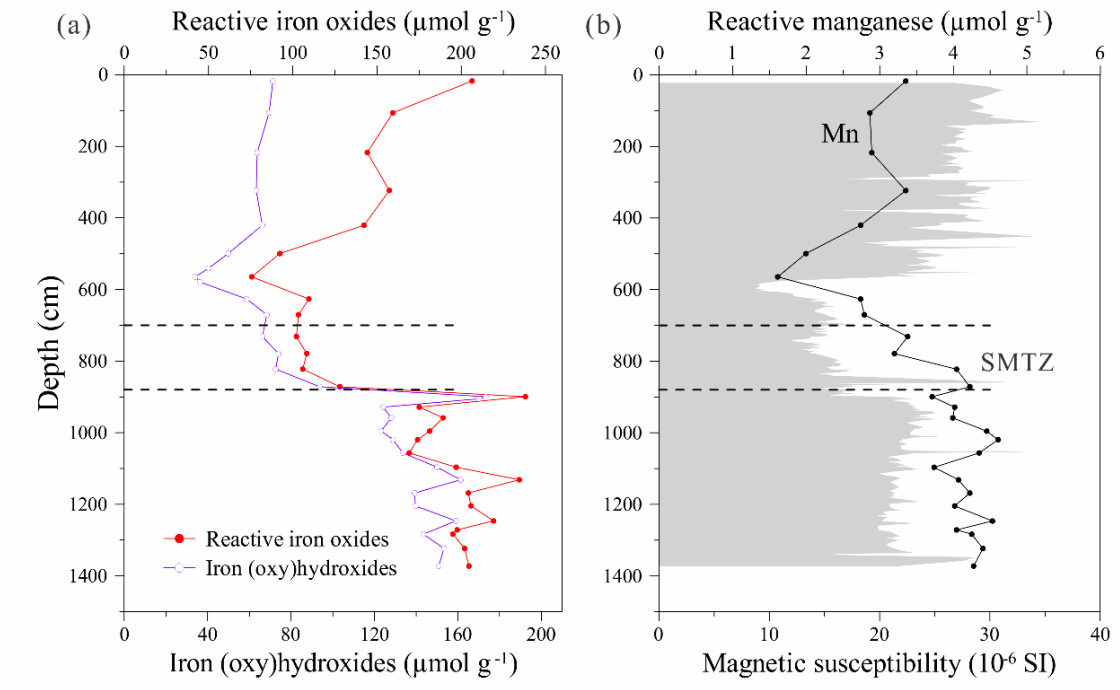

Figure 8: Depth distribution profiles of (a) Fe (oxy)hydroxides and reactive Fe-oxides, (b) reactive manganese and magnetic susceptibility. Magnetic susceptibility data are adopted from Lin et al. (2017a).

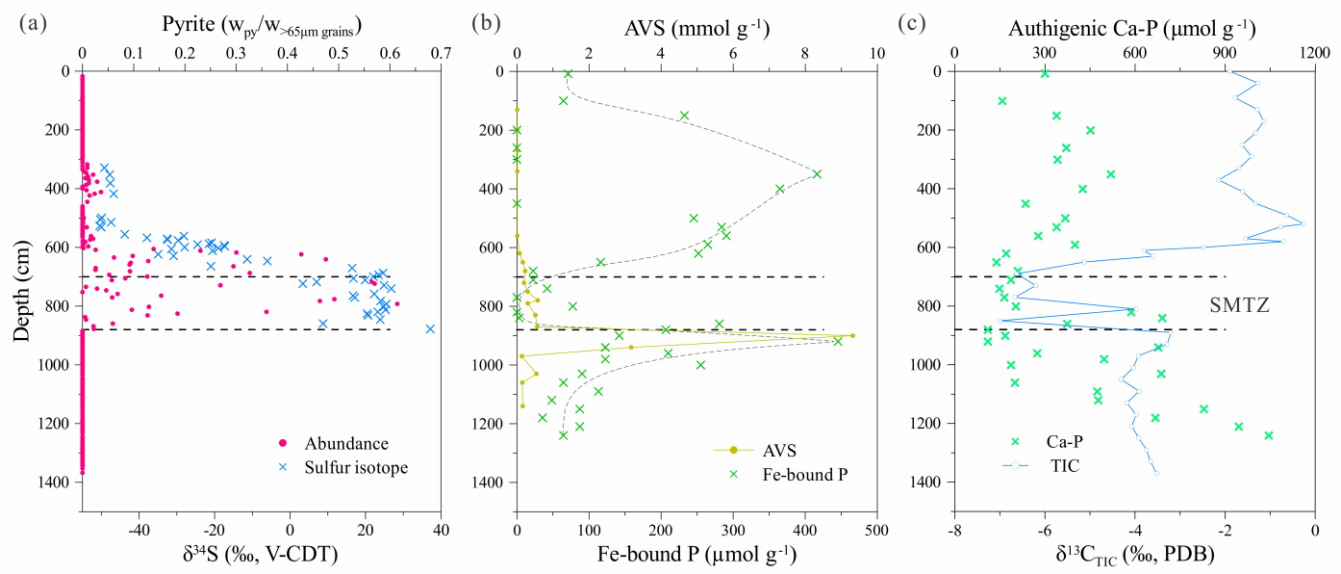

Figure 9: Depth profiles of (a) handpicked pyrite abundance and sulfur isotopic composition (Lin et al., 2015), (b) acid volatile sulfur (AVS) and Fe-bound P (Zhang et al., 2014, 2018b), (c) authigenic Ca–P and carbon isotopic composition of total inorganic carbon (TIC) (Ou, 2013; Zhang et al., 2018b, 2018c).

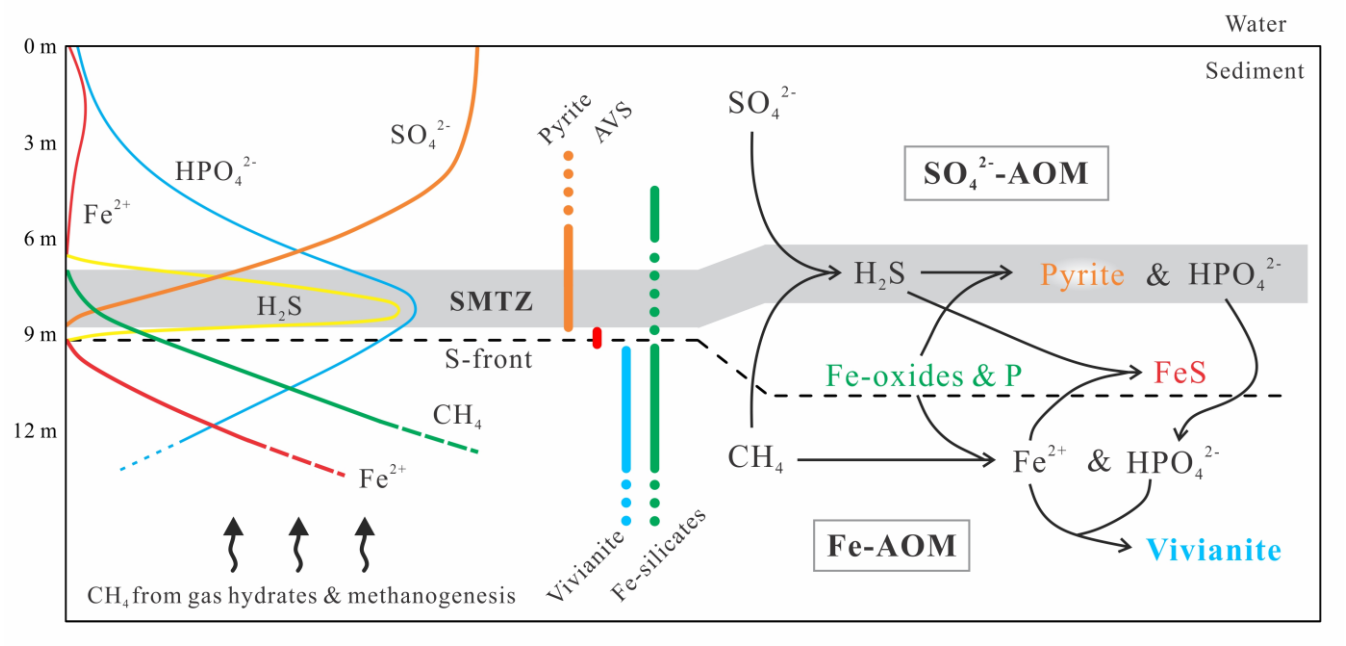

Figure 10: Schematic representation of vivianite formation below the SMTZ at Site 973-4 in the South China Sea. The left and middle parts illustrate idealized pore water and solid-phase mineral distributions. The right part illustrates the interaction between sulfate- and Fe-driven AOM coupling Fe-S-P-CH_4 cycles in proximity to the SMTZ.